ARCHER

Collaborative Project

Co-funded by the European Commission under the
Euratom Research and Training Programme on Nuclear Energy
within the Seventh Framework Programme

Grant Agreement Number: 269892
Start date: 01/02/2011Duration: 48 Months

www.archer-project.eu

Experimental results of dust mobilization with the BISE facility

Samuel Peillon (IRSN), François Gensdarmes (IRSN), Audrey Roynette (IRSN)

ARCHER project–Contract Number: 269892
Advanced High-Temperature Reactors for Cogeneration of Heat and Electricity R&D
EC Scientific Officer: Dr. PanagiotisManolatos

Document title	Experimental results of dust mobilization with the BISE facility
Author(s)	Samuel Peillon (IRSN), François Gensdarmes (IRSN), Audrey Roynette (IRSN)
Number of pages	39
Document type	Deliverable
Work Package	WP2.3.3
Document number	D23.33– revision 0
Issued by	IRSN
Date of completion	30/09/13
Dissemination level	Restricted to the partners of the ARCHER project

Summary

The present document is the final milestone of the task 2.3.3 (WP23) for the **ARCHER project** (Advanced High-Temperature Reactors for Cogeneration of Heat and Electricity R&D) of the 7th Framework Programme. In the framework of HTR nuclear safety, it is fundamental to assess the potential for dust mobilisation in case of an accidental leak of the primary circuit (risk of explosion, spread of contamination). For this purpose, the characterization of dust mobilization is mandatory. The aim of this final report is to provide dust mobilization data on a small-scale IRSN facility named BISE and located in Saclay (France).
The BISE facility used for particle resuspension experiments was presented in a previous report (WP2.3.3, D23.31). The present report introduces results obtained with the test matrix defined in the report WP2.3.3, D23.32 but also concerns the parameters identified as playing a significant role in particle resuspension. Indeed, one can find within this document all resuspension fractions that have been measured and calculated for a total of 227 experiments. After global considerations on these results and an estimation of the spread of data, the phenomenology of resuspension is discussed. Data are then compared with two different resuspension models available from the literature by means of a semi-empirical correlation. Finally, it is proposed to develop a suitable correlation with its own domain of validity and adapted to our results.

Approval

Rev.	Short description	First author	WP Leader	SP leader	Coordinator
0	First issue	Samuel Peillon (IRSN) 30/09/13		Norbert Kohtz (TUV – Rheinland) 03/10/13	Sander De Groot (NRG) 03/10/13

Distribution list

Name	Organisation	Comments
P. Manolatos	EC DG RTD	
All technical participants	ARCHER	
Steering Committee members	ARCHER	

Table of contents

List of figures

List of tables

1 Introduction

In the framework of HTR (High Temperature Reactor) nuclear safety, it is fundamental to assess the potential for dust mobilisation in caseof an accidental leak of the primary circuit (risk of explosion, spread of contamination). For this purpose, the characterization of dust mobilization is mandatory. The aim of this final report is to provide dust mobilization data on a small-scale IRSN facility named BISE and located in Saclay (France) for future code qualification.
In reports WP2.3.3, D23.31 (Gensdarmes and Roynette, 2011) and WP2.3.3, D23.32 (Peillon *et al.*, 2012), we presented the characteristics of the BISE facility (Alloul, 2002) and the method followed in carrying out experiments with it. We chose to study the case of a heap of powder submitted to airflow because we noticed a lack of knowledge for this geometry. Indeed, the case of thin multi-layers deposit is quite well understood and described by the so-called Rock'n roll model from Reeks & Hall (2001). Thus, in the case of an accumulation of particles in a dead zone (elbow pipes, etc.), we expect to have deposits with different geometries and not thin layers of particles. Experiments were done with alumina powders identified at the laboratory as surrogate of graphite dust we may find in HTR. These powders are easier to manipulate and can be found in great quantities. Attention was given to the main surrogate parameter, i.e. the particle size distribution regarding HTR dust. More data can be found in report WP2.3.3, D23.32.
We chose to follow an experimental design (see WP2.3.3, D23.32) which allowed to limit the number of tests, while maximizing the amount of information that could be derived from each tests. We also noticed that many parameters are involved in the resuspension process. So, we propose, in first instance, to identify those of greatest importance for resuspension. The results of this study are presented in this report. We also present the results of all the experiments (227 in total) undertaken, notably the resuspension fractions which resulted from this series of tests. We then compare these with other studies in the literature on resuspension. In particular, we will see similarities and differences which can be identified relative to a specific empirical relationship, but also relative to a theoretical model which is currently used in some computational codes.

2 Experimental Methodology

2.1 First considerations

The conduct of an experiment in the BISE facility, from the initial preparation of the different materials used in the tests, up to the weighing of the test surface after the experiment, can be split into three main steps.

- One should first manually adjust, and measure by means of anemometry, the various parameters relating to air flow (speed, acceleration).

- The second step is to make, weigh and introduce into the test facility the powder cone on its test surface (this step can be repeated several times if we consider that the deposit is not consistent).

- Finally, the experiment itself is begun. After being exposed for a period Δt determined by experience, the deposit of powder remaining on the test surface is extracted from the facility and weighed.

Hence, an experiment of this type extends over a period of about 3 hours, of which the actual exposure time of the deposit is 15 min.

To avoid potential systematic errors (a "time" effect) in the analysis due, for example, to a change in the level of an uncotrolled factor between two sets of experiments (drift in a measuring instrument), the experiments are performed in a random order. Thus, the systematic error is also made random: the measurement uncertainty is increased, but this does not skew the result.

Once the experiments have been completed in accordance with the Plackett-Burman design matrix (see Report WP2.3.3 D23.32 - Table 4.1), we carry out a statistical analysis of the results. This allows to assess the relative effects of parameters on the resuspension fraction, $K_{R.}$

Figure 1 shows the histogram of the effects of each parameter on the resuspension fraction, $K_{R.}$ This histogram is known as a "Pareto chart".

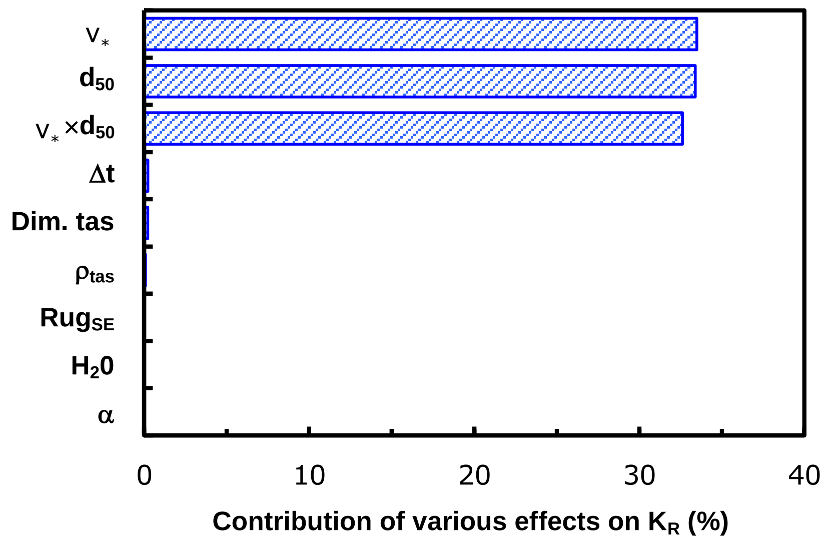

Figure 1 - Contribution of various effects on K_R - Analysis of the Plackett-Burman screening plan, type 12.11p (Report WP2.3.3, D23.32 - Table 4.1)

The analysis of the effects clearly shows that the friction velocity (v_*) and particle median diameter make a very significant contribution, much higher than the other six factors considered. They each contribute to more than 30% of the overall effect, and so these two parameters play an important role in resuspension. The other six parameters do not have a significant effect on K_R in the experimental conditions of the screening design. However, given the small range of variation of some parameters, caution is warranted as to their true importance.

Because of the very low contribution of the other six parameters, the strong interaction effect between friction velocity and particle median diameter is highlighted. This also contributes to about 30% of the overall effect on the resuspension fraction.

From these experimental results, we can then develop a linear statistical model (a simple mathematical tool) which expresses the resuspended fraction as a function of the free-stream velocity and particle median diameter. This statistical model is used only to assess the change of K_R with respect to these two factors, in no way does it allows one to calculate a value for the resuspension fraction. The resulting model, shown in three dimensions in Figure 2, takes into account the two-factor interaction between the free-stream velocity and the particle median diameter. Our experimental results are shown as circles in Figure 2.

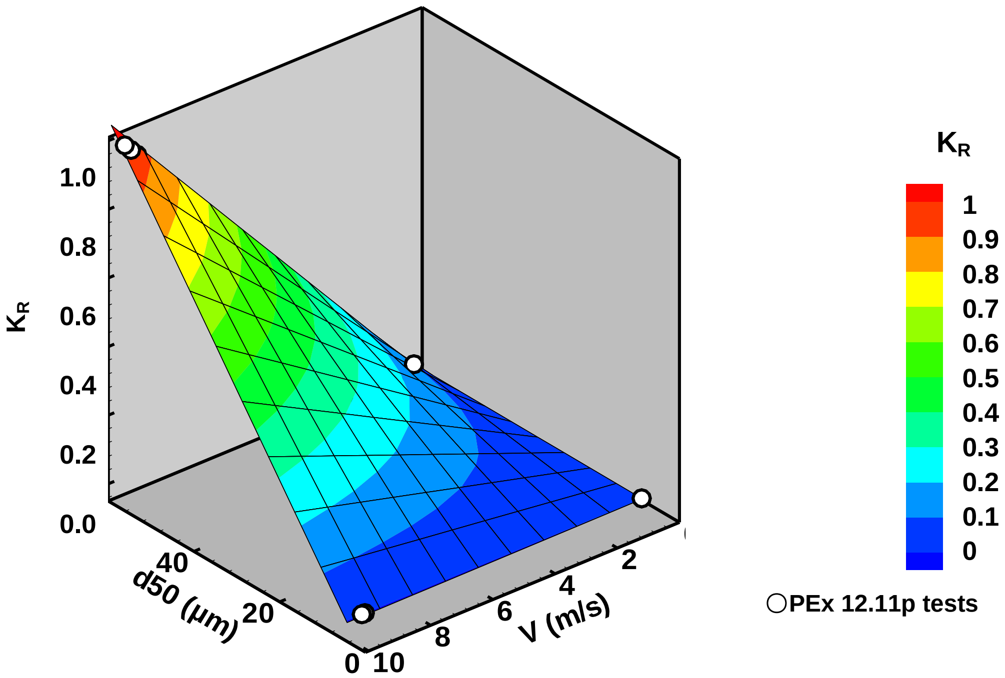

Figure 2 - K_R (d_{50}, v): Statistical model obtained from the Plackett-Burman 12.11p design

Figure 2 shows the interaction between the parameters, free-stream velocity and particle-size distribution. It was found that the effect of velocity on K_R differs depending on the powder size. The effect is positive, becoming more important as the particle-size distribution increases.

One can also notice that our experiments, carried out according to the experimental design 12.11p, lie at the four corners of the experimental space. The model developed from these data therefore gives no information as to what might occur between the two levels studied (whether the response is linear or non-linear).

Following this first series of experiments, it seemed that a special study of the effects of free-stream velocity and particle-size distribution on the resuspension fraction was needed to describe more accurately how K_R changes within the study region. Using five parameter levels, the 13.2p design (Report WP2.3.3 D23.32 - Table 4.3) statistically identifies a quadratic model of K_R as a function of free-stream velocity and particle-size distribution. We note again that this is just a simple mathematical model that only allows to observe parameter trends, not to predict the values of K_R.

This model is obtained from the analysis of all the data (pooling the experimental results from the 12.11p and 13.2p designs). It is shown in Figure 3 as a two-dimensional projection of K_R onto the (d_{50}, v_*) plane. We also show the experimental results from the two designs.

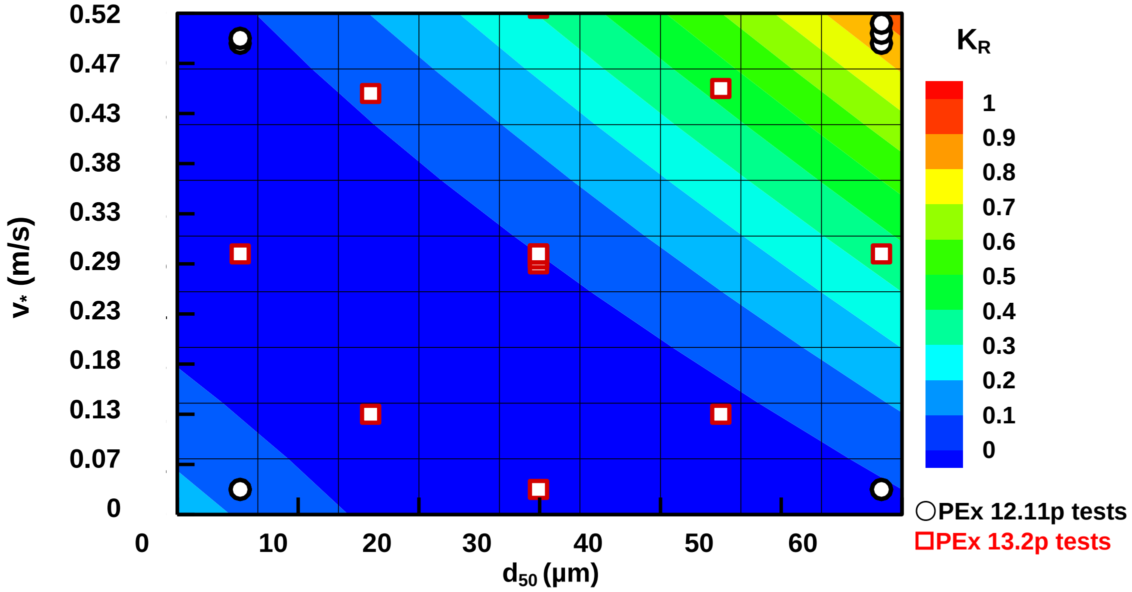

Figure 3 - Illustration of the of 2D quadratic model of K_R as a function of the particle median diameter d_{50} and the friction velocity v_*, obtained from the data points of the 12.11p and 13.2p designs

This analysis shows that resuspension is a threshold phenomenon. From Figure 3 we observe that, for a constant particle-size, resuspension occurs only above a certain critical friction velocity which corresponds to a threshold friction velocity. Theoretically, resuspension always occurs (assuming a distribution of adhesion forces). However, in our experiments, the resuspension process is not measurable below our detection limit.

The observed friction velocity threshold depends obviously on particle size distribution. According to the statistical model fitted to our experimental data in Figure 3, resuspension begins to be detectable only at a friction velocity of about 0.38 m/s (corresponding to a free-stream velocity of 7 m/s in BISE) for a d_{50} of 20 microns. On the other hand, at 40 microns, one can detect resuspension once the friction velocity reaches 0.21 m/s (or V = 3.5 m/s). So, as the particle size increases, the threshold friction velocity decreases. This threshold friction velocity is thus inversely proportional to the powder's particle-size distribution.

Moreover, we note that for a powder with a median diameter of less than about 5 microns and at low friction velocity, the model attributes a higher value to K_R than for powders of larger sizes. This can be explained by the fact that particles clump together and form larger diameter aggregates which are then resuspended. However, the d_{50} shown on the graph corresponds to the median diameter of the powder used in the experiments, and not to the size of any aggregates which are formed and resuspended. Thus, we consider this as an artifact of the experiment.

2.2 The different phases of resuspension

The screening study of the influence of friction velocity and particle size distribution was conducted by carrying-out a large number of additional experiments in the intermediate zones of change, where we had few data. As a result, we can now describe more precisely how the resuspension fraction changes as a function of these two parameters. Since the aim of this work is to develop a semi-empirical model of the resuspension process, it is necessary to be able to collect a large number of results to give a consistent data base upon which we can rely.

Integrating the Plackett-Burman design experiments into our analysis (and treating the six non-significant parameters as having negligible effects on the experimental results), we finally carried out a hundred experiments. The experimental data correspond to 27 different configurations of the couple (v_*, d_{50}). Figure 4 shows our complete results. In it, we display, on a linear scale, the average resuspension fractions $\overline{K_R}$ as a function of the friction velocity for five selected particle size distributions of Al_2O_3 powder. These averages were obtained from a variable number of tests (from 2 to 18 data points), depending on the experimental configuration. For the sake of legibility, we have not shown the confidence intervals about the means in this figure. These, however, have been discussed in Report WP2.3.3 D23.32 - paragraph 2.

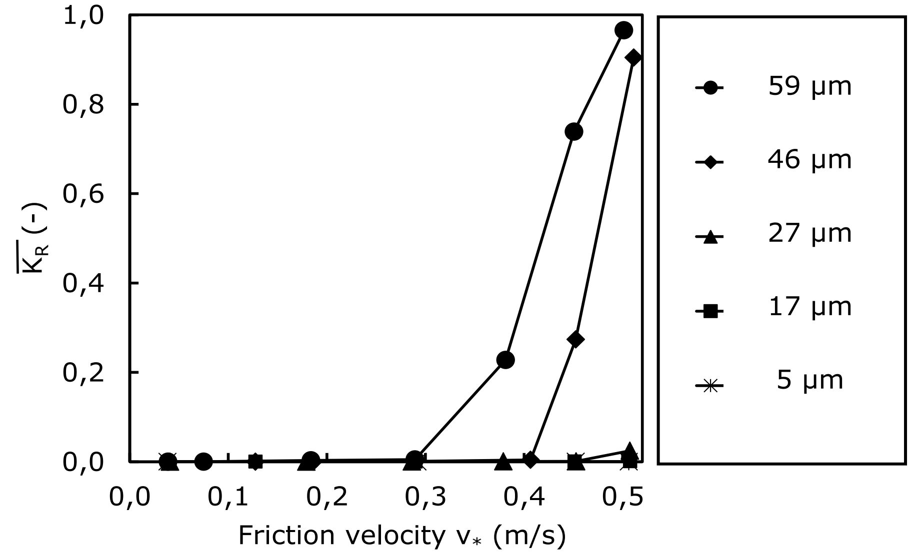

Figure 4 - Changes in the average resuspension fraction as a function of the friction velocity for different particle size distributions of alumina powder

This figure clearly shows the previously observed threshold effect. We also note that, for a given friction velocity, the resuspension fraction, K_R, is greater when the particle size distributions are large. This result is consistent with the physics of adhesion in our experimental domain.

In addition, Figure 4 shows that the use of a linear scale doesn't allow to precisely describe the resuspension process, especially at low friction velocities. In Figure 5, we show the same results on a logarithmic scale $\overline{K_R}$. Each graph describes the experimental averages $\overline{K_R}$ obtained for a specific particle size distribution, as a function of the air friction velocity. Our mean values, usually based on three experiments, are presented here with 95% confidence intervals.

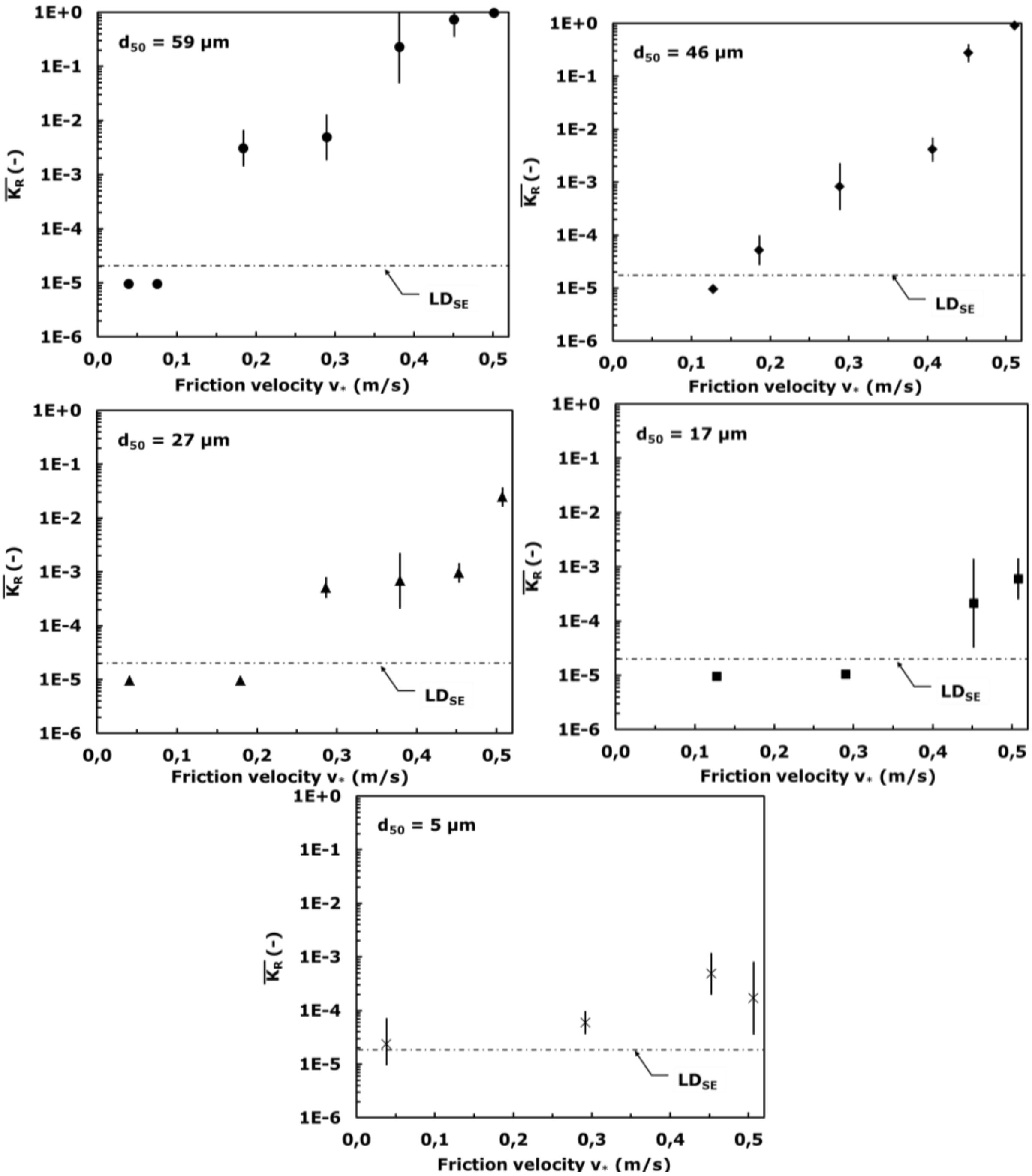

Figure 5 - Resuspension fractions as a function of the friction velocity v_* for Al_2O_3 powders with d_{50} equal to 5, 17, 27, 46 and 59 microns - Average values are displayed with their 95% confidence intervals

This logarithmic scale representation is more suited for describing the resuspension since, as can be seen from these graphs, the values of $\overline{K_R}$ covers the range of 10^{-5} to 1 (i.e., 6 orders of magnitude). In the remainder of our study, we will base the analysis of our results on log $K_{R.}$

The lower limit (horizontal dotted line on the graph) corresponds to our detection limit LD_{SE}. Therefore, when the measured $\overline{K_R}$ becomes greater than LD_{SE}, we consider that the velocity threshold is crossed. From Figure 5, it is possible to determine a velocity range corresponding to this threshold. However, this interval is specific to our facility and our measurement method: the threshold determined is in fact a pseudo-velocity under which the resuspension fraction is below our detection limit. Thus, regardless of the particle size distribution, no resuspension is measured with our system for a friction velocity $v_* \leq 0.07$ m/s (or $V \leq 1$ m/s). However, the latter increases when the particle size distribution decreases.

The study of our experiments confirmed by the results of Figure 5 leads to conclude that the resuspension of a conical deposit occurs in two main phases.

The first concerns the resuspension fractions for which $\overline{K_R}$ is less than about 10^{-3} - 10^{-2}. Under these conditions, we attribute the resuspension to particles positioned on the surface of the deposit; these are directly exposed to the incoming air flow. This resuspension process, similar to the case of resuspension of a flat multi-layer deposit, is said to be "superficial". Thus, it must be independent of the shape of the deposit. The second phase is associated with fractions greater than about 10^{-2}. Above this value of K_R, the deposit is deformed under the action of the high free-stream velocity. We will discuss this in more detail in § 4.

The transition between these two phases occurs over a relatively narrow velocity range which depends on the particle size distribution. These different phases are shown in Figure 6 for the case of resuspension of a 46 microns powder deposit. They are delimited by dotted lines. The area of overlap between the "superficial" and "distortion" phases is attributed to the transition zone.

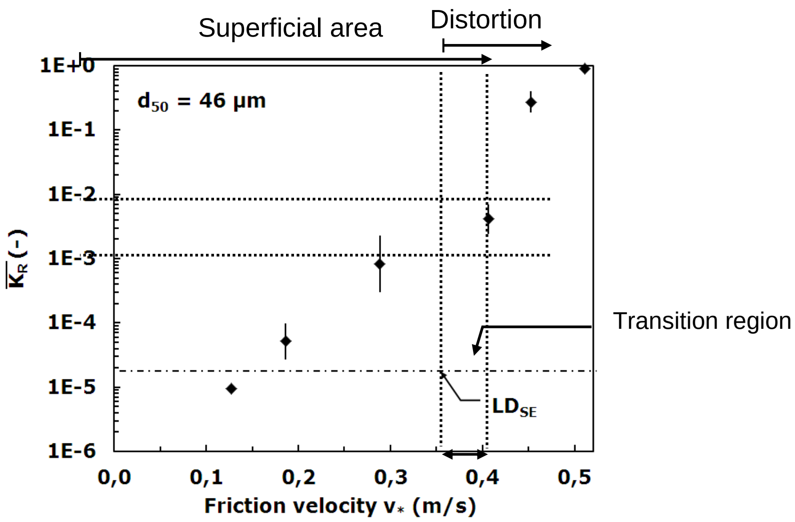

Figure 6 - Changes in the average resuspension fraction for particle sizes of 46 microns as a function of friction velocity - Identification of the transition zone

Under our experimental conditions, we can observe the transition zones for powders whose median diameters are between 27 and 59 microns. For smaller particle size distributions, the maximum fraction reached is of the order of 10^{-3} in the BISE velocity range. Thus, only the "superficial" resuspension phase takes place.

Table 1 shows the limits of the free-stream velocities characterizing the transition zones of the different powders deriving from the analysis of our results.

Table 1 - Limits of air velocities characterizing the transition zone

d_{50} (µm)	Limiting velocity (m/s)			
	Lower		Upper	
	v_*	V	v_*	V
17	> 0.5	> 10	n/a*	n/a*
27	~0.45	~8.5	~0.50	~10
46	~0.40	~7.5	~0.45	~8.5
59	~0.30	~5.0	~0.38	~7.0

As can be seen from this table, these limits are a function of the size of the resuspended particles. Note that the distortion phase is more applicable for large particle sizes.

Finally, analysis of the confidence intervals in Figure 5 shows that the variance of the resuspension fraction values depends on the experimental setup. So, in the course of our study, we endeavored to consistently repeat the same test three times. The standard deviation calculated from these three experiments gives us an estimate of the true standard deviation of our measurements.

3 Overall analysis and variability in the results

Based on our whole set of experiments, we attempt to generalize the relative effects of the eight parameters studied across our entire experimental domain. We then describe the experimental variation across all our studies.

3.1 Overall assessment on the effects of the studied parameters

We performed a multiple linear regression for all our experimental data. The resulting analysis of this database, which consists of 227 experiments (see Appendix 1), allows us to assess the relative influence of eight resuspension parameters studied across the whole experimental domain of BISE. Table 2 summarizes the different effects of these parameters and outlines the areas of study for which these factors were studied:

Table 2 - Classification of parameters and BISE experimental domains

	Parameters	EXPERIMENTAL DOMAIN
PRIMARY	Friction velocity	0.04 to 0.52 m/s (0.5 ≤ V ≤ 10 m/s)
	Median particle diameter of Al_2O_3 powder	5-59 microns (σ_g = 1.3)
SECONDARY	Moisture content of the powder	0 and 1 mg H_2O/g
	Airflow acceleration*	0.3 to 31 m/s^2
NOT SIGNIFICANT	Exposure time	30 sec to 60 min
	Pile shape	Cone - truncated pyramid - disc
	Surface roughness	0 - 12.5 µm
	Tap density of powder	1.5 to 2 g/cm^3

*Effect related to exceeding the average speed

Thus, this analysis allows us to confirm the fundamental influence of the so-called "primary" parameters, i.e., the friction velocity and particle size distribution, as well as their interaction. It also allows to appraise, across the experimental domain, two "secondary" parameters. These are the moisture content of the powder and the acceleration at the start of the flow. These two parameters have a significant influence on resuspension, after the primary effects of the velocity and particle size distribution have been accounted for, under certain conditions which we will discuss. We note however that:

- The moisture content of the powder has a negative effect on resuspension.
- Beginning at a threshold value of the acceleration, the resuspension fraction increases with acceleration. In fact, this increase is due to above-average instantaneous free-stream velocity during the acceleration ramp. This particular acceleration effect is therefore specific to the BISE facility and the experimental conditions.

Finally, the results of our multiple regression show that four of the eight parameters studied do not have a significant influence on resuspension. These are the exposure time, the pile shape, the surface roughness and the powder density. Among them, however, are two parameters which have a very localized effect on the suspension. These are the time of exposure, whose effect dies away after 15 minutes, and the pile shape which arises only from a characteristic deformation rate of the deposit, and this only over a limited range of free-stream velocity. However, given the strong influence of the primary and secondary parameters, the effects of exposure time and pile shape are not significant in our experimental conditions.

3.2 Standard deviations of the results

To assess the uncertainty of our measurements, which is mainly related to the variability arising from successive weighings, we calculated the measurement standard deviation $\sigma(\log K_R)$ obtained in each test, using equation (2.5) of Report WP2.3.3 D23.32. These standard deviations are shown as a function of log K_R in Figure 7.

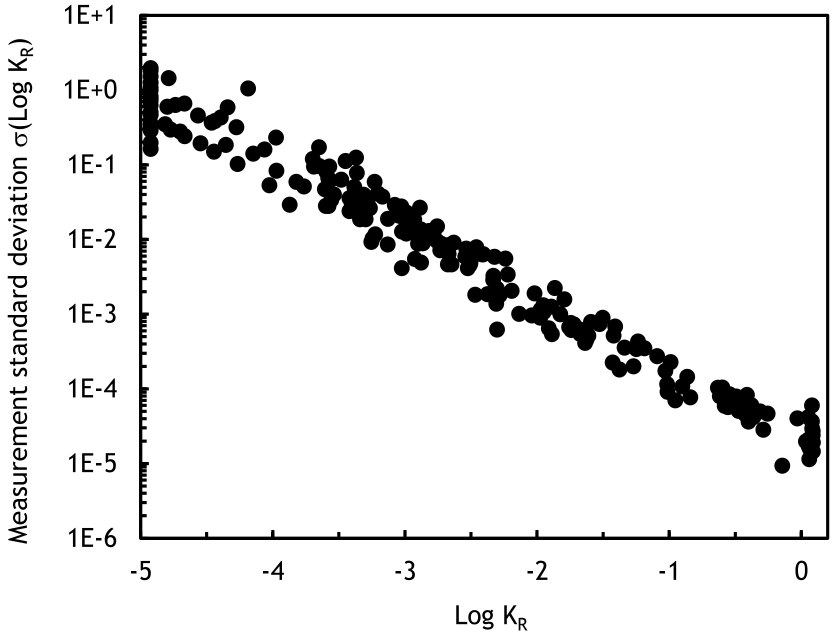

Figure 7 - Plot of the experimental standard deviation measurements versus the values of the logarithm of the resuspension fractions K_R from the experiments

The results in Figure 7 show that the higher the resuspension fraction, the lower the measurement uncertainty. The 227 experiments are divided into 73 different experimental configurations. Repeated measurements have been made on each configuration (between 1 and 18 repetitions, depending on the configuration). For each, we calculate the experimental standard deviation $\sigma'(\mathrm{Log}K_R)$, using relationship (2.9) of Report WP2.3.3 D23.32. These standard deviations are plotted in Figure 8 against their averages.

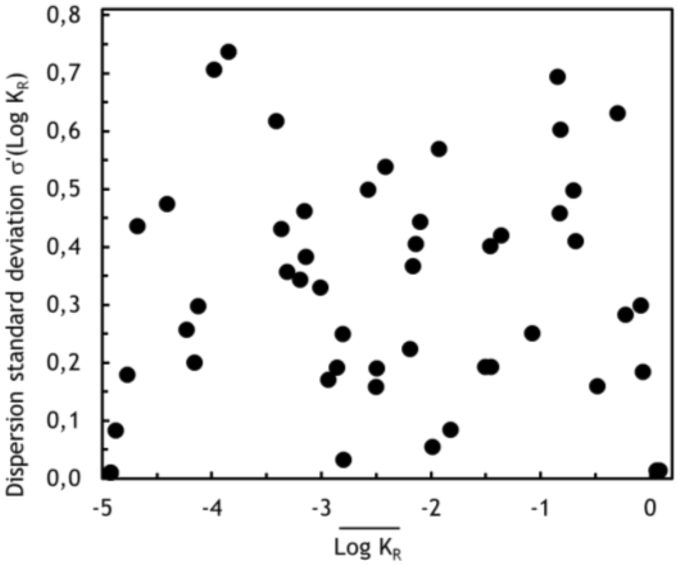

Figure 8 - Plot of the experimental standard deviations against the average values of the logarithm of the resuspension fractions from the experiments

Figure 8 shows that these observed experimental standard deviations are random. One sees, in fact, that the variance of the results is independent of the average value of K_R and therefore of the phenomenon of resuspension. However, since the standard deviations are relatively homogeneous, we can determine an average experimental standard deviation σ_{exp} (relationship 2.10 - Report WP2.3.3 D23.32) having a pooled degree of freedom which is the sum of the degrees of freedom of the individual standard deviations. This leads to $\sigma_{exp} = 0.41$. This standard deviation has a degree of freedom ν_{exp} = 154. We can then compare the different measurement standard deviations with the average experimental standard deviation σ_{exp}. Figure 9 plots the percentage values of the variance ratios as a function of K_R.

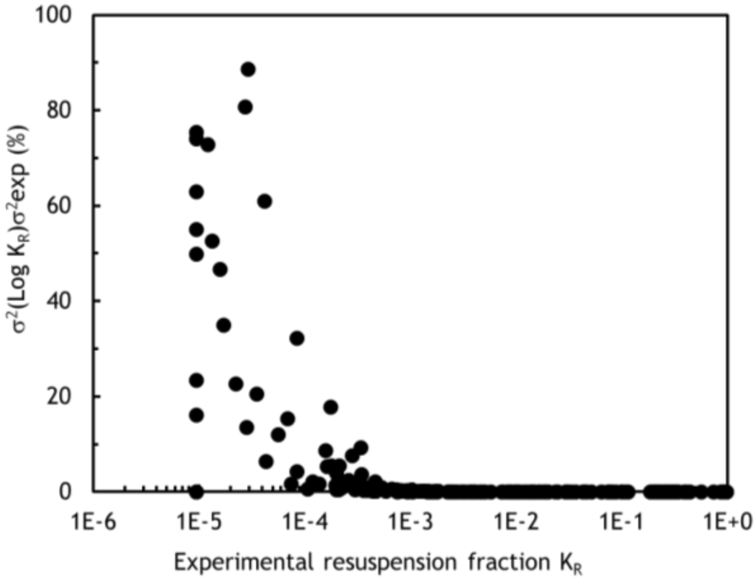

Figure 9 - Percentage values of the ratios of measurement variance to the average experimental variance plotted against the experimental resuspension fraction

This graph shows that for low values of K_R (close to the detection limit), the variance associated with the measurement is very important relative to the experimental variance.

However, when $K_R \geq 10^{-4}$, less than 5% of the experimental variance is attributable to the weighing procedure. Under these conditions, the variability of the results largely arises from the phenomenon of resuspension. Finally, from the uncertainty relating to $2\,\sigma_{exp}$ on log $K_{R,}$ we can estimate the experimental uncertainty obtained in the resuspension fraction. Thus log $K_R \pm 2\ \sigma_{exp.}$

This gives values for the maximum (K_{Rmax}) and minimum (K_{Rmin}) resuspension fraction:

$$K_{Rmax} = 10^{0.82} \times K_R = 6.60 \times K_{R,}$$

and

$$K_{Rmin} = 10^{-0.82} \times K_R = 0.15 \times K_R.$$

We increase these results to:

$K_{Rmax} = 10 \times K_{R,}$

and

$K_{Rmin} = 0.1 \times K_R$.

The average uncertainty in all of our experimental results is determined at the 95% confidence level to ± 1 order of magnitude. We use this interval in the data analysis and the establishment of the relationship in paragraph 5.

4 Description of resuspension

Following on from these results, and with a view to understanding the phenomenon of resuspension, we are interested in how the particles of a pile of powder go into resuspension. The purpose of this section is not to study the deformation of a pile of powder and describe its physics. That forms a whole study in its own right (Foucault, 1994; Dauchot *et al, 2001;* Andreotti *et al, 2002).* Here, we focus specifically on the phenomenology of the deformation phase, a phase that has been demonstrated for resuspension fractions greater than about 10^{-2}, as well as how it changes over time. The majority of our experiments were performed with conically shaped deposits, which is why we give particular consideration to the resuspension process for this type of pile. However, we also compare the observed phenomena with deposits shaped as a truncated pyramid or a disc.

4.1 Deformation of conical deposits

To facilitate the observation of resuspension, some experiments were filmed in BISE with a SONY (XC-8500 CE) digital camera. A first sequence of photographs is shown in Figure 10. It shows the change over time of the resuspension of a cone of alumina powder with particle size of d_{50} = 59 microns and exposed to a friction velocity of v_* = 0.52 m/s (V = 10 m/s). The sequence was taken from above the deposit, the air flows from left to right in the pictures. One can distinguish the circular test surface on which the powder is deposited.

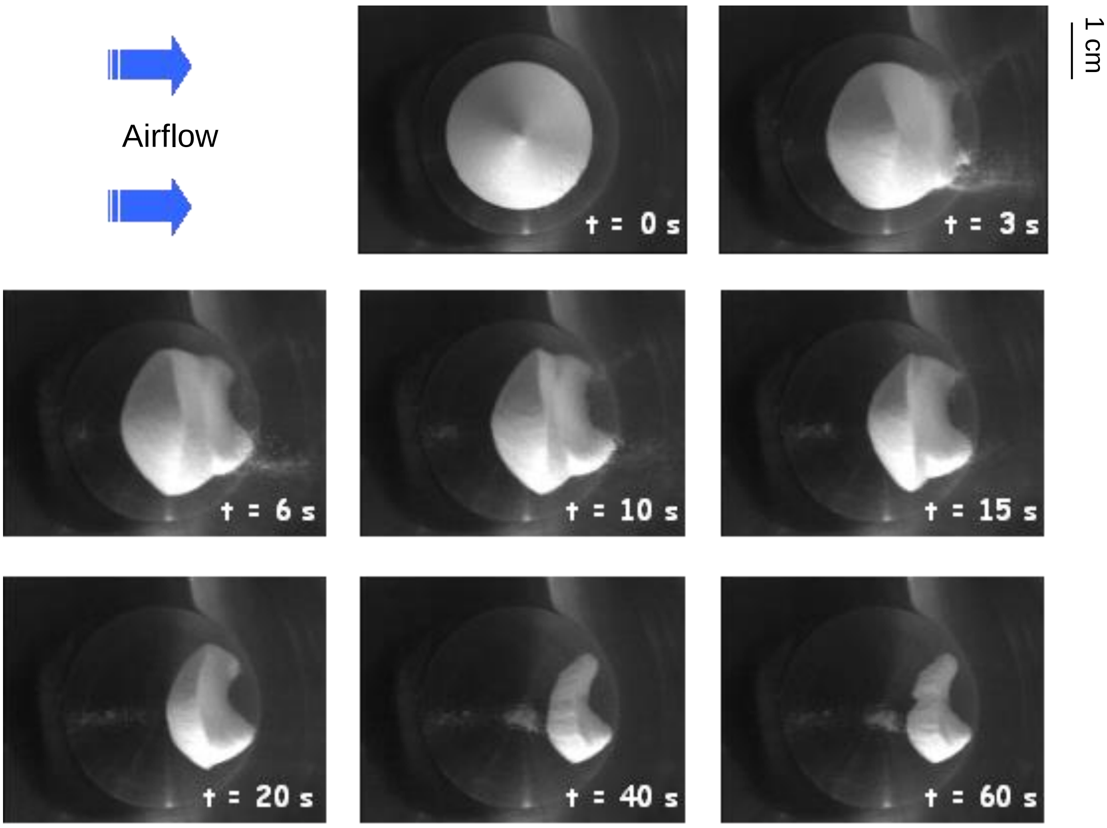

Figure 10 - Sequence of photographs showing changes in a conical deposit of Al_2O_3 powder as a function of time (d_{50} = 59 microns and v_* = 0.52 m/s (V = 10 m/s)) - K_R = 9.7x10^{-1}

This sequence of photographs shows that, under these experimental conditions, resuspension primarily happens during the first forty seconds. After that, the resuspension is stable. Thus, beyond a few tens of seconds, we observed experimentally that the exposure time has no further influence on the phenomenon. Here, for Δ t = 2 min, we obtain K_R = 9.7x10^{-1}.

In addition, Figure 10 shows the complexity of the phenomenon of resuspension. Indeed, combined with the more detailed analysis of our results, it confirms the hypothesis that resuspension occurs in two concurrent phases, one of which is governed by a so-called "superficial" suspension process which is analogous to a multi-layer deposit which takes place during the first few seconds, and a second phase that only begins above a certain friction velocity which causes a deformation of the pile of powder (this speed being reached after 0.3 s in Figure 10). As it is clearly seen, this deformation phase involves two resuspension phenomena, the first localized on the surface facing the incident air flow, the other localized on the pile's rear face. That is why we divide resuspension into what happens upstream and downstream of the pile, our goal being to identify the relative importance of these two phenomena, using the ordered pair (v_* , d_{50}).

Indeed, upstream of the deposit there is a development of the boundary layer along and parallel to the surface of the cone: the friction velocity v_* of the incident air therefore increases from the base to the top of the pile. Accordingly, the number of particles mobilized is larger at the top than at the base of the pile, since the particles at the top are exposed more rapidly to their threshold speed. Therefore, this phenomenon leads to a reduction in the height of the pile, as the photos in Figure 10 show. It is thus responsible for the shape taken by the front of the deposit as time progresses. As for the upstream particles which are not at the top of the cone, but whose threshold speed is reached, they are driven by the flow lines around the pile.

We also note the appearance of a deposit of particles aligned along the principal axis of air flow. This alignment appears with disappearance of the pile upstream (pictures t = 6 s to t = 60 s in Figure 10). Two hypotheses are suggested to explain this phenomenon:

- the existence of a stalling point (V = 0 m/s) in the main flow axis located at the base of the upstream face of the pile of powder,
- the existence of micro-vortices upstream which resuspend the particles.

However, the latter hypothesis seems the more plausible because we have measured turbulence intensity of the order of 20% at the base and upstream of the pile, which would make vortices here quite likely. Similarly, we distinguish here:

- the shear layer that begins at the top of the cone: it is conceivable that this shear layer creates small vortices; downstream, the formation of these vortices would increase the velocity of the particles located at the top, and the movement of such particles would become greater than upstream; this assumption is realistic because the picture at t = 15 s in Figure 10 shows that the top of the heap on its downstream side widens, while, upstream, the pile becomes round.
- the air recirculation zone, formed by a big vortex: different photographs of Figure 10 show that the vortex must move in all three spatial dimensions; in this zone of low-pressure and sheltered from the wind (the y-axis speeds are close to zero and turbulence is high), one can imagine that the separation of the particles is caused by suction due to the pressure gradient.

One also notes at the downstream side of the pile's base, two "smears" of particles symmetrically placed with respect to the main y-axis flow. Two hypotheses have been advanced as to their origin.

These particles come from:

- a saltation (movement of particles by leaps and bounces) of the largest particles coming from upstream,
- a deformation due to the vortices in the wake of the pile (sliding of large particles on the downstream side due to the flight of smaller particles swept along in the vortex).

We took another sequence of photographs on Al_2O_3 powder of diameter d_{50} = 27 microns and with a friction velocity of v_* = 0.52 m/s (V = 10 m/s). The only parameter that has changed between the experiment of Figure 10 and that of Figure 11 is the smaller particle size distribution.

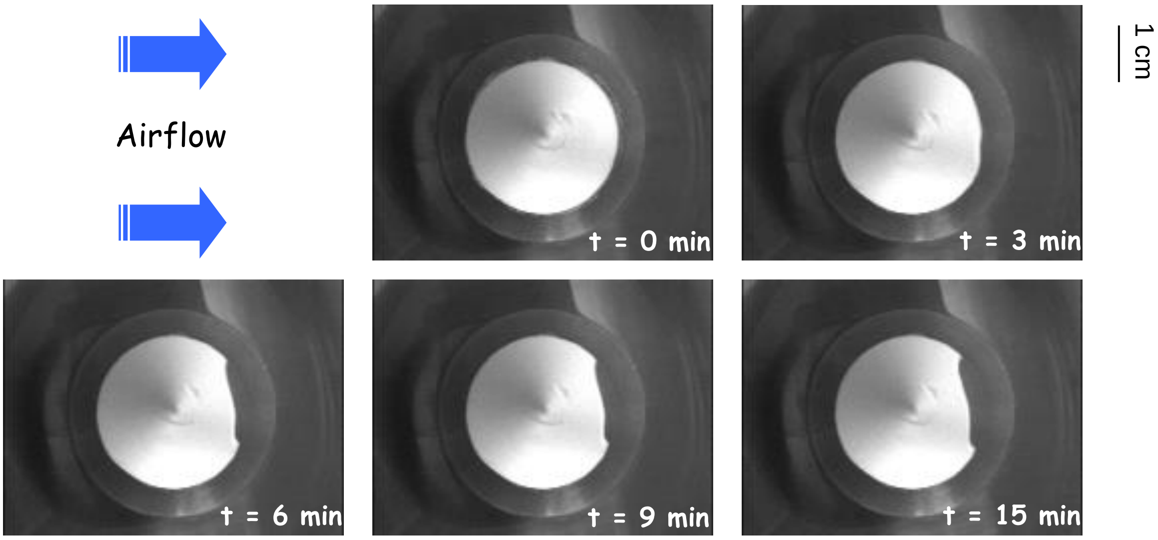

Figure 11 - Sequence of photographs showing changes in a conical deposit of Al_2O_3 powder over time (d_{50} = 27 microns and v_* = 0.52 m/s (V = 10 m/s)) - K_R = 4.0x10^{-2}

From this series of pictures, and in these experimental conditions, we can see that the resuspension (now lower because K_R = 4.0x10^{-2}) behaves differently from those experiments where d_{50} = 59 microns (see Figure 10):

- the deformation of the deposit is slower: visually, the resuspension process seems hardly to have started after 3 min. However, the deformation is observed once 1% of the initial mass of powder has been resuspended (or K_R = 10^{-2}). Thus, although qualitatively the resuspended mass appears to increase more significantly between t = 3 min and t = 6 min, this increase actually only corresponds to a change of less than one order of magnitude (after 15 min, only 4% of the original mass had been suspended);
- only the downstream phenomenon exists and differs from the experiment of Figure 10: the air recirculation zone is present. On the other hand, it seems that the shear layer at the top of the pile does not exist, because the summit was not in any way deformed. Further experiments performed under the same experimental conditions confirm this hypothesis.

Finally, although the particle size distributions are smaller in this case, the movement phenomena observed here strongly resemble studies conducted in the field of wind transport of particles: moving dunes in the desert (Bagnold, 1941), phenomena of flight of material under the effect of wind erosion (Foucault, 1994), simulation of the formation and movement of dunes in the laboratory (Dauchot *et al., 2001;* Andreotti *et al*., 2002). However, we note that the mechanisms of resuspension, especially those related to particle size distributions, are different.

4.2 Deformation of other types of deposit

By the way of comparison, we present two experiments carried out on alumina powders of d_{50} = 46 microns at a friction velocity of 0.52 m/s (V = 10 m/s). The first is the resuspension of a deposit having a truncated pyramid shape and other a disc-shaped deposit.

With reference to this particle size distribution and with a friction velocity of 0.52 m/s, the conical deposit only deforms downstream (see Figure 11). However, after 15 min, there is a crescent moon on the surface, corresponding to K_R ~ 9x10$^{-1.}$
It is found that the resuspension of a pile of powder in the shape of a truncated pyramid behaves similarly to a cone. However, the sequence of photographs in Figure 12 shows that the deformation of a truncated pyramid is far more complex than that of a cone:

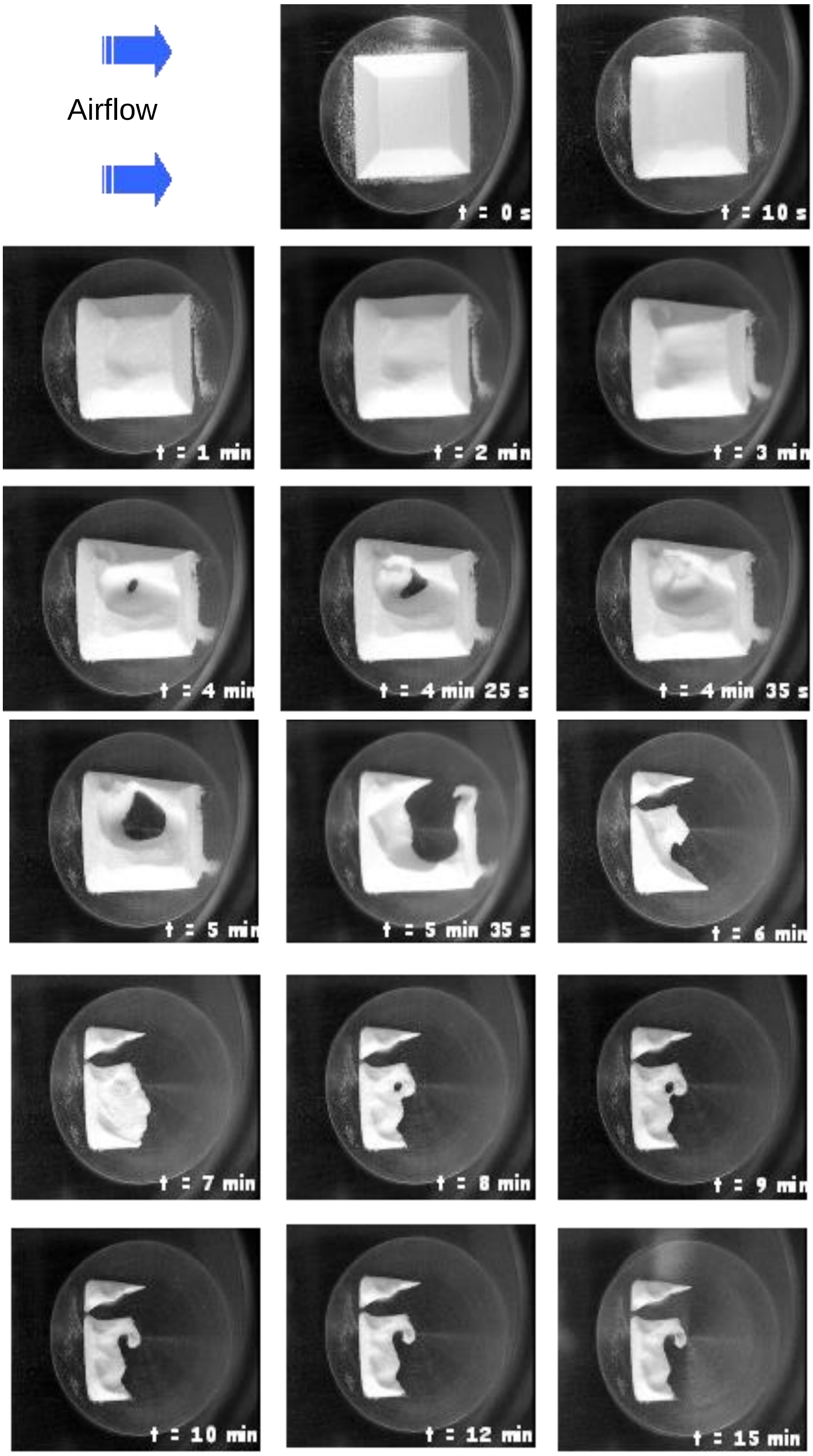

Figure 12 - Sequence of photographs showing changes in a truncated pyramid deposit of Al_2O_3 powder over time (d_{50} = 46 microns and v_* = 0.52 m/s (V = 10 m/s)) - $K_R = 6.3x10^{-1}$

From these photographs, the majority of resuspension takes place downstream of the deposit. One observes the presence of a very large shear zone that begins on the upstream edges of the deposit. Particles located on these edges are then resuspended, resulting in a rounding of the truncated pyramid. The phenomenon is even more pronounced in that the edges of the truncated pyramid facing the flow "disappear" after the first few seconds (pictures t = 0 s and t = 10 s in Figure 12).

In addition, the boundary layer which develops along the upstream surface must undergo a separation when it arrives at the high base of the truncated pyramid, resulting in the production of a wake. One can imagine that the presence of intense vortices at this level will dig into the center of the pile and act as in the recirculation zone to resuspend the particles (pictures t = 4 to t = 5 min).

Finally, the recirculation zone is present but its effect is less than in the previous phenomenon. In the first five minutes, one sees clusters of particles accumulating in a crescent downstream of the pile, like for a cone of 59 microns powder (see Figure 11). After this exposure period, the two phenomena eventually merge, consequently resuspending the entire downstream side of the deposit.

The sequence of photographs in Figure 13 shows the evolution of resuspension of a deposit of d_{50} = 46 microns powder in a disc shape, exposed to a free-stream velocity of 10 m / s.

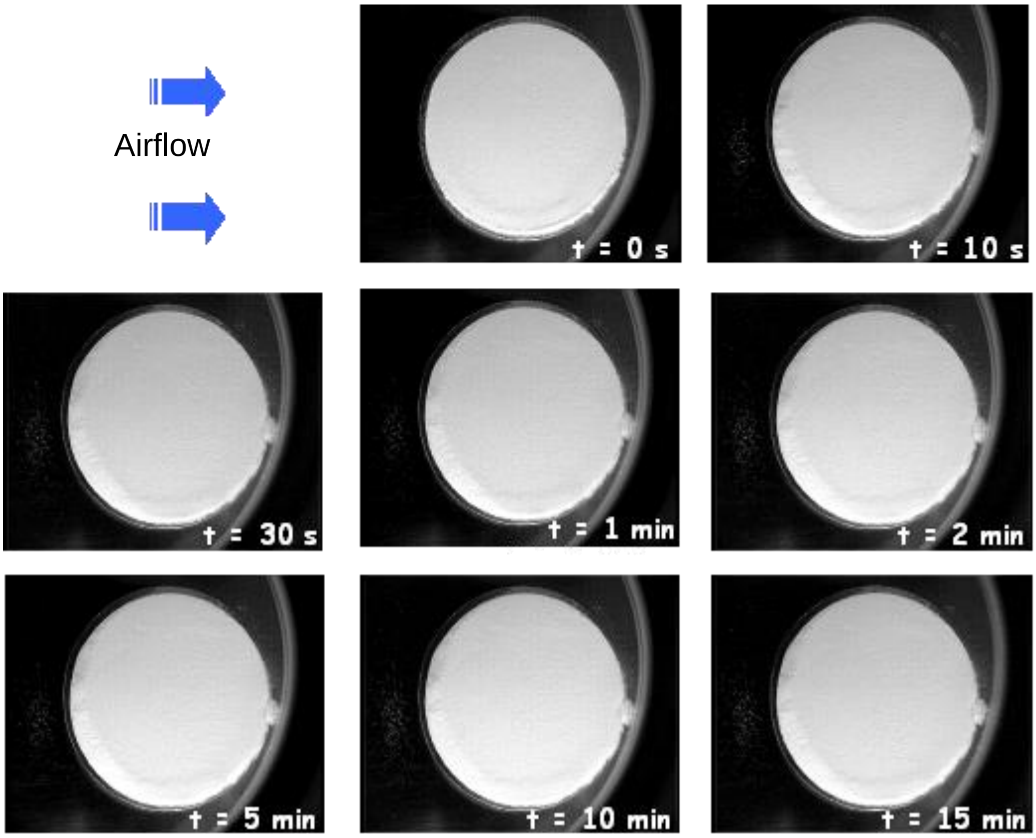

Figure 13 - Sequence of photographs showing changes in a disc-shaped deposit of Al_2O_3 powder over time (d_{50} = 46 microns and v_* = 0.52 m/s (V = 10 m/s)) - K_R = 7.3x10^{-2}

It was found that the resuspension of the disc exposed to a speed of 10 m/s led to a much smaller resuspension fraction than the previous two shapes with the same d_{50}: K_R here is 7.3x10^{-2} at Δt = 15 min. However, in comparison to other shapes studied, the resuspension visually appears to be much less, the fraction measured remains in the range ± an order of magnitude which corresponds to the estimate made of the variability in our results. In addition, the photographs of Figure 13 clearly show that, in these conditions and for this shape, the deformation phase has hardly begun after 15 min. So, one only sees, on the upstream side, a rounding of the top of the disc, and this occurs in the first few seconds. This is due to the presence of high shear at the edges directly exposed to the air flow. Indeed, most of the particles in this type of deposits are completely embedded in the viscous sub-layer of the boundary layer.

All these photographic sequences show how complex the phenomenon of resuspension of a pile of powder is. Depending on the initial experimental conditions, especially those of free-stream velocity, particle size distribution and the shape and/or structure of the deposit, we find there are many particle flight phenomena.

These particles detach themselves from the pile, whether from its downstream side (sheltered from the incident air flow), its upstream side (facing the incident air), or from both sides. In addition, the effects of turbulence differ from one situation to another, making the descriptions of the phenomenon very complicated.

However, these observations are very informative. Firstly, they allow to confirm that resuspension happens in two phases. Secondly we can validate the very small influence on the resuspension fraction of parameters such as exposure time or the shape of the deposit, taking into account the variability of our results.

We now have accumulated enough experimental data to compare them with some existing models in the literature. Note, however, that variety of experimental conditions in the literature and the complexity of the phenomenon of resuspension, leads to suspect that the existing models will not allow to correctly describe the suspension conditions for our pile of powder. If this turns out to be the case, the development of a specific relationship would then appear to be necessary.

5 Development of a semi-empirical relationship

Our literature review revealed two models that seem particularly promising for comparison purposes. These are the resuspension model of Fromentin (1989) and the rock 'n' roll model of Biasi *et al.* (2001). The first, developed from experimental results carried out on multi-layer deposits is a macroscopic description of the resuspension process. The second is based on a mechanistic description of the resuspension of a particle deposited on a rough surface (Reeks and Hall, 2001). The latter was adapted and validated in tests of both mono-layer and multi-layer deposits. We thus compare our data with these two models.

5.1 Fromentin's empirical relationship model (1989)

Using data derived from multi-layer deposits of powders having a diameter between about 0.5 microns and 5 microns, which were exposed to free-stream velocity of 5 m/s to 25 m/s in the PARESS experiment (either $0.23 \leq v_* \leq 1$ m/s), Fromentin (1989) derived a semi-empirical model of the resuspension flux, as a function of the exposure time Δt and friction velocity at the wall v_*. This relationship is only applicable for $v_* \geq 0.29$ m/s and does not include the effect of the particle size distribution parameter. Figure 14 shows our data for particles having median diameters from 5 microns to 27 microns as a function of the K_R calculated from the fitted relationship for the friction velocities measured in BISE for 10 m/s. Our data are shown with 95% confidence intervals. Those calculated using the Fromentin model are presented with an uncertainty of $\pm$ an order of magnitude. This confidence interval is the one defined by A. Fromentin himself.

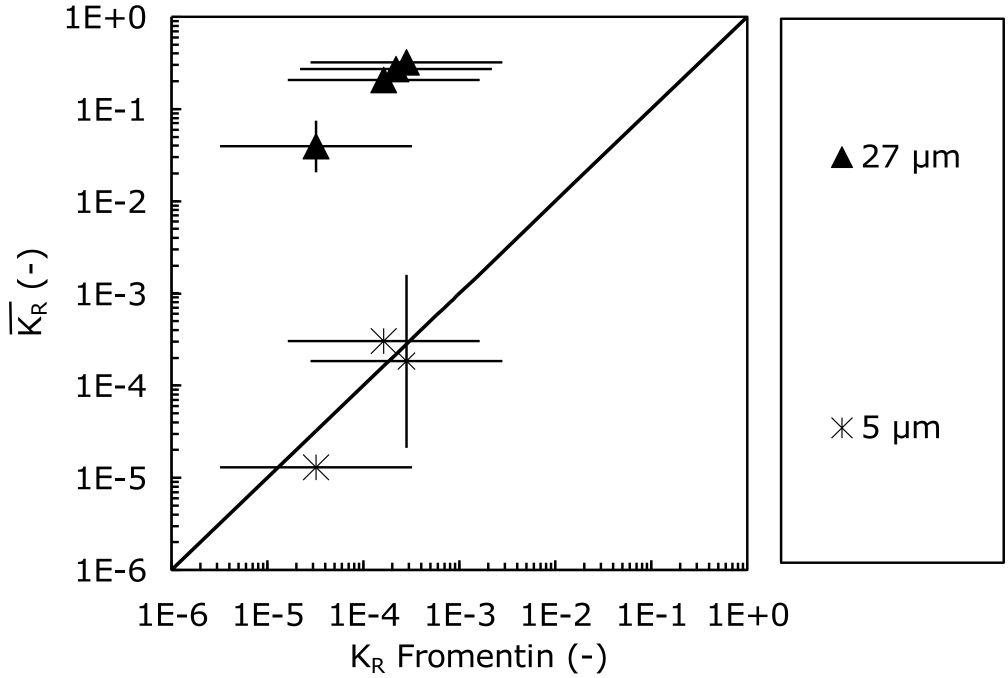

Figure 14 - Average fraction resuspended in BISE (v_*= 0.52 m/s (V = 10 m/s), and d_{50} = 5 and 27 microns) as a function of the resuspended fraction using the Fromentin relationship (1989)

Given the conditions of validity of the model, Figure 14 shows that our results appear to be in good agreement with the Fromentin relationship for small particle size distributions. For powders of d_{50} = 5 microns, our experimental points between about 10^{-5} and 5 x 10^{-4} are approximately of the same order of magnitude as the Fromentin model predictions for slightly finer particles (K_R between 5 x 10^{-5} and 5 x 10^{-4}). However, under these experimental conditions, we observed that resuspension is due to the appearance of larger size clusters. Since Fromentin's conditions are close to ours, it is likely that the same phenomenon occurred in his experiments. However, Fromentin does not take account of this in his relationship and attributes the calculated resuspension flux to the sizes of the original particles.

On the other hand, when the particle sizes become greater than those used by Fromentin, the relationship no longer holds. Indeed, for a particle size of d_{50} = 27 microns, the results in Figure 14 show that our experimental data and the model differ by 2-3 orders of magnitude. The fact that the relationship does not take into account the effect of particle size distributions therefore makes this model difficult to use.

In addition, for an air friction velocity less than 0.29 m/s or 5 m/s in BISE, our method allows to measure the resuspension fraction for several particle size distributions. However, these results cannot be determined from the Fromentin relationship because the author incorporated the threshold speed used in PARESS (v_* = 0.29 m/s), a value which, as we have already pointed out, depends on the detection limit of the measurement technique used. So, this further reduces the scope of the Fromentin relationship.

5.2 Rock 'n roll model

The second model to compare with our experiments is based on a detailed analysis of resuspension that takes into account the phenomenon of "tilting - rolling" (Rock 'n roll) around a surface irregularity to describe how a particle detaches itself from a rough surface (Reeks and Hall, 2001). This approach suggests that resuspension is a quasi-static phenomenon, especially considering that after one second, the resuspension hardly changes.

This Rock 'n roll model has recently been used to interpret several sets of experimental data in the literature. The correlated model thus obtained (Biasi *et al.,* 2001) allows the validation of the original model for particles size distributions between 0.1 and 30 microns, and for two types of deposits, mono-layer and multi-layer. As a result, the authors suggest that the type of deposit should be omitted from the resuspension phenomenon.

Figure 15 provides a description of the tipping movement/rotation of an isolated spherical particle in contact with two asperity points, P and Q, where the surface is irregular, as defined in the Reeks and Hall model (2001).

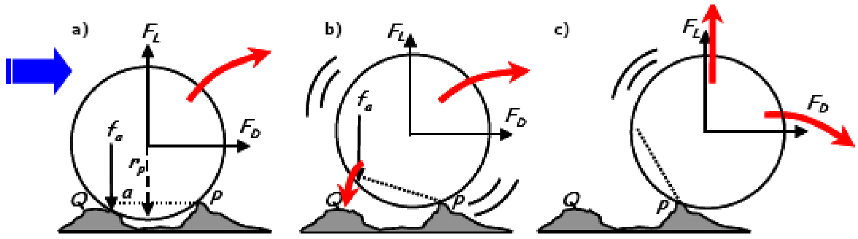

Figure 15 - Movement of tilting/rolling in the rock 'n' roll model

The different stages of movement can be describe as follows:

a) the particle rests on both of the asperity points, held by the action of adhesive forces,
b) oscillations of the particle around the point P due to the drag torque - a lift which tends to sweep it away in the air flow, counteracted by the two adhesive forces that tend to keep it on the surface,
c) the particle has accumulated enough rotational energy to break contact with the asperity point P. It can then lift (if $F_L > F_D$ - unlikely) or start rolling away (if $F_D > F_L$ - very likely) after breaking contact.

To mathematically describe this model, the authors assume a Gaussian distribution of the aerodynamic forces F_R and a log-normal distribution of the normalized adhesive forces $\varphi(f_a^{'})$.
The latter are written:

$$\varphi\left(f_a^{'}\right) = \frac{1}{\sqrt{2\pi}}\left(\frac{1}{f_a^{'} \ln \sigma_a^{'}}\right)\exp\left\{-\frac{1}{2}\left[\frac{\ln(f_a^{'}/\overline{f_a^{'}})}{\ln \sigma_a^{'}}\right]^2\right\}, \quad (5.1)$$

where:

$f_a^{'}$: Normalized adhesive force (f_a/F_A, with $F_A = \frac{3}{2}\pi \cdot \gamma \cdot r_P$ being the adhesive force of a spherical particle upon a smooth surface), γ is the surface energy and r_p is the particle radius,

$\overline{f_a^{'}}$: Geometric mean of normalized adhesive forces,

$\sigma_a^{'}$: Geometric standard deviation of the distribution of the adhesive forces.

The gravity force is neglected. The authors then propose an expression for the suspension rate $p(f_a)$ (in s^{-1}) for particles subject to the adhesive force f_a:

$$p(f_a) = n_\theta \exp\left[\frac{-(f_a - \overline{F_R})^2}{2\sigma_R^2}\right] \Big/ \frac{1}{2}\left\{1 + \text{erf}\left[\frac{f_a - \overline{F_R}}{\sqrt{2}\sigma_R}\right]\right\}, \quad (5.2)$$

where:

$n_\theta = 0{,}00658 \times \left(v_*^2 / \nu\right)$: resonant frequency of particle-surface system,

v_*: friction velocity of the gas at the wall,
ν : kinematic viscosity of the gas,

$f_a = f_a^{'} \cdot F_A$: adhesive force,

$\overline{F_R}$: average of the aerodynamic forces,

σ_R : standard deviation of the distribution of the adhesive forces.

The fraction K_R of the resuspended particles is thus given by:

$$K_r\ (\Delta t) = 1 - \int_0^\infty \varphi\left(f_a'\right) \cdot \exp\left[-p\left(f_a\right) \cdot \Delta t\right] \times df_a', \tag{5.3}$$

where Δt represents the exposure time.

Based on the results from a large number of resuspension experiments, Biasi *et al.* (2001) determined the best-fit pairs $\overline{f'_a}$ (the reduction of adhesive forces compared to the smooth case) and σ'_a (the spread in adhesion). They then develop relationships between the geometric mean adhesive force $\overline{f'_a}$ and the geometric standard deviation σ'_a of the particle diameter d_p measured in microns. These relationships are written as:

$$\overline{f'_a} = 0.016 - 0.0016 \times d_p^{0,545} \tag{5.4}$$

$$\sigma'_a = 1.8 + 0.0515 \times d_p^{1,4}. \tag{5.5}$$

Figure 16 presents the first results of the analysis using the correlated model of Biasi *et al.* (2001). It describes the average resuspended fraction $\overline{K_R}$ as a function of the friction velocity v_*. We have presented here our mean experimental results from BISE for particle sizes of 17 and 59 microns, together with their 95% confidence intervals and the values of resuspended fractions calculated using the Biasi *et al.* model(2001).

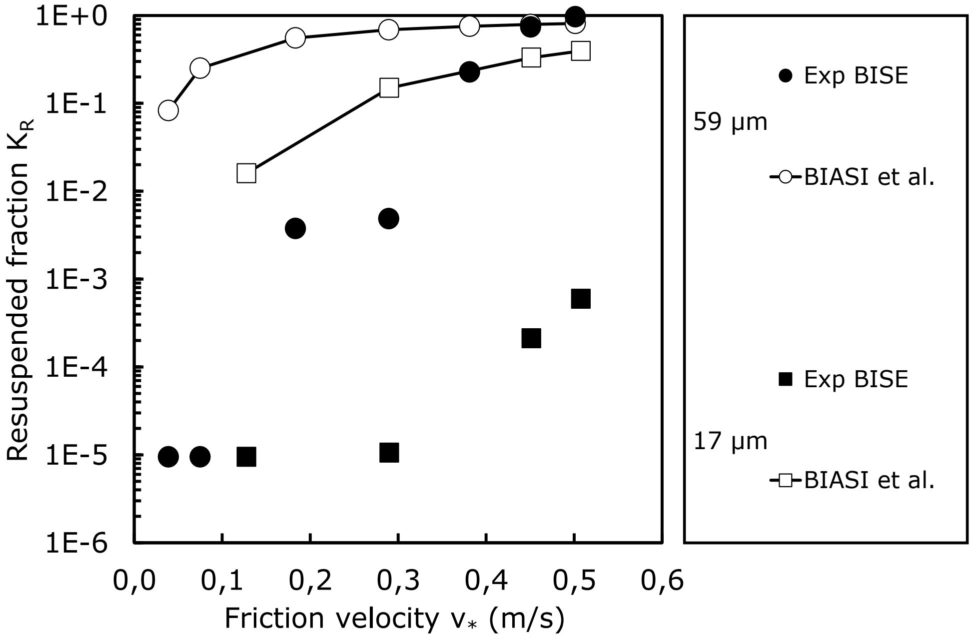

Figure 16 - Comparison of the BISE experimental results with the Biasi *et al.* (2001) model as a function of the friction velocity for powder deposits with d_{50} = 17 and 59 microns

Note that the model of Biasi *et al.* (2001) does not agree with our results and systematically overestimates our data. The observed bias is even more important at lower values of our measured fraction. This gap can reach four orders of magnitude for the lowest friction velocities. This is explained by the fact that the relationships describing the distributions of adhesion forces have been established by the authors from data which resulted in high values of K_R. Therefore, for values of K_R less than 10^{-1}, this model does not correctly describe the resuspension we observe.

To analyze whether the rock 'n' roll model can nevertheless better represent our data, we tried to develop relationships between the geometric mean of the adhesion strength $\overline{f'_a}$ and its geometric standard deviation σ'_a, these being fitted to our experimental results in BISE. To do this, we adopted the same approach as Biasi et *al.* (2001). Obtaining these relationships was thus carried out in three steps:

1) For these two data sets, we vary the values of $\overline{f'_a}$ and σ'_a systematically, until the K_R derived by the Rock'n roll model is closest our data. In this way, we get a pair $\left(\overline{f'_a},\ \sigma'_a\right)$ for each particle size distribution, which allows the rock 'n' roll model to describe our experiments better. The rock 'n' roll model derived for d_{50} = 59 microns and 17 microns with these new pairs is shown in Figure 17, as a function of the friction velocity. For comparison, we also plotted our experimental points for both particle size distributions on the graph.

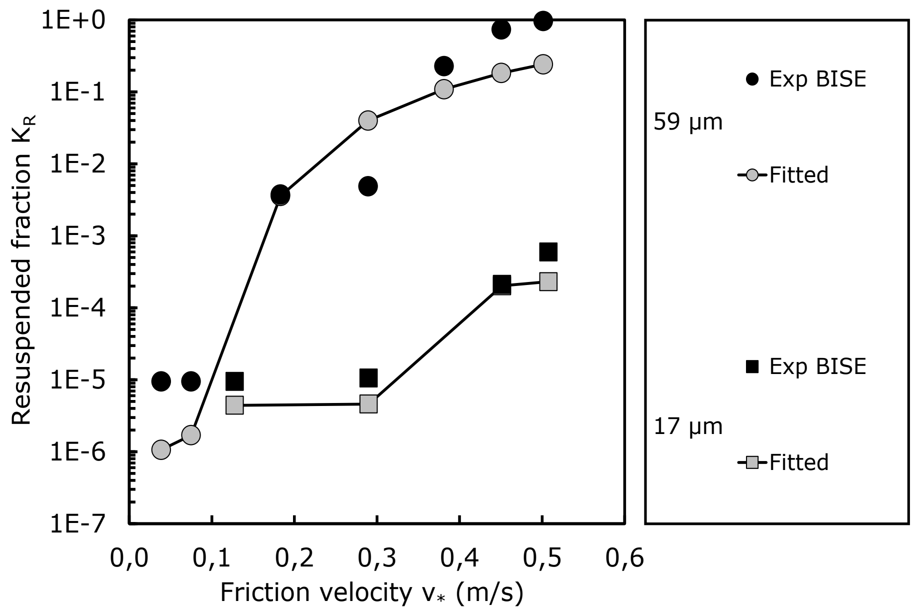

Figure 17 - Comparison of BISE experiments with the fitted Biasi *et al.* (2001) correlation for powder deposits of d_{50} = 17 and 59 microns

Figure 17 shows that the model calculated with our pairs of values $\left(\overline{f'_a},\ \sigma'_a\right)$ is better fitted to our experimental data than the model of Biasi et *al.* (2001) described in Figure 16.

2) We then apply the same process to all our data. Figure 18 shows the results calculated from the pairs of values $\left(\overline{f'_a},\ \sigma'_a\right)$ found for each particle size distribution. It also shows the results obtained for the 17 and 59 microns powders in Figure 17. We see here the values of K_R calculated with the Biasi *et al.* (2001) model, and those obtained by fitting our data, as a function of the mean resuspended fraction obtained experimentally in BISE for the different particle size distributions studied. The limits shown indicate ± an order of magnitude relative to those defined in § 3.2.

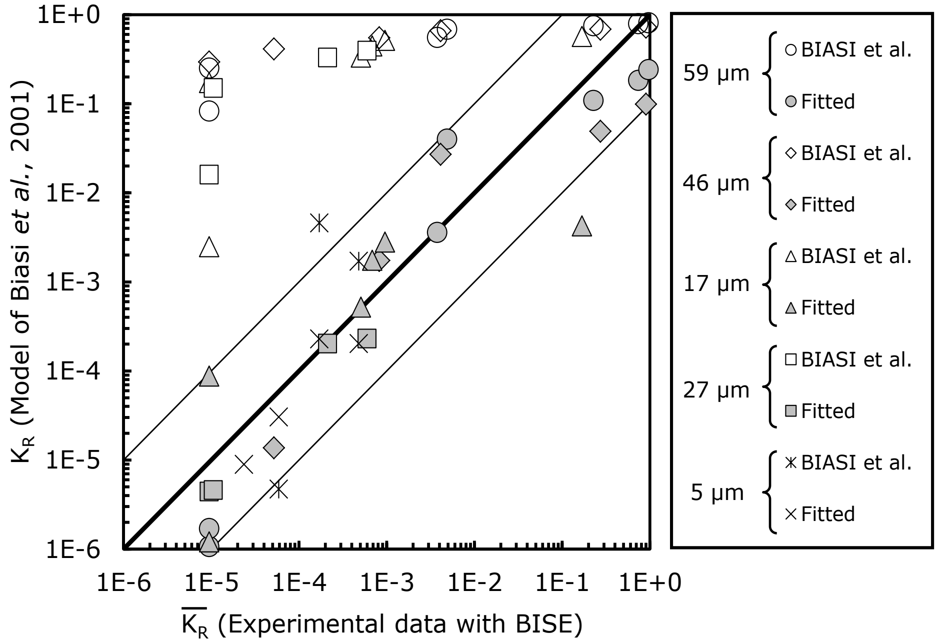

Figure 18 - Comparison of the BISE experimental results with the correlated model of Biasi *et al.* (2001) and the fitting of this model carried out in BISE

This graph confirms the initial trends seen in Figure 16:

- Only the values of $K_R > 10^{-1}$ are adequately represented by the model of Biasi *et al. (2001).*
- Below this value, the model overestimates our data by up to four orders of magnitude.

We note, however, that the experimental data obtained for d_{50} = 5 microns are those for which the correlated model of Biasi *et al.* (2001) fits best.

Furthermore, the results of fitting the BISE data show that resuspended fractions calculated from the five pairs of values $\left(\overline{f'_a},\ \sigma'_a\right)$ found make it possible to significantly improve the rock 'n' roll model. The K_R values calculated in this way are practically all within ± an order of magnitude of our experimental values.

3) From the five pairs $\left(\overline{f'_a},\ \sigma'_a\right)$ obtained, we thus investigate if a relationship can be defined as a function of particle diameter. To do this, we represent in Figure 19 our fitted values of $\overline{f'_a}$ (Left graph) and of σ'_a (Right graph) as a function of the particle median diameter. By the way of comparison, we add the relationships $\overline{f'_a}$ and σ'_a of Biasi *et al.* (2001)to each graph.

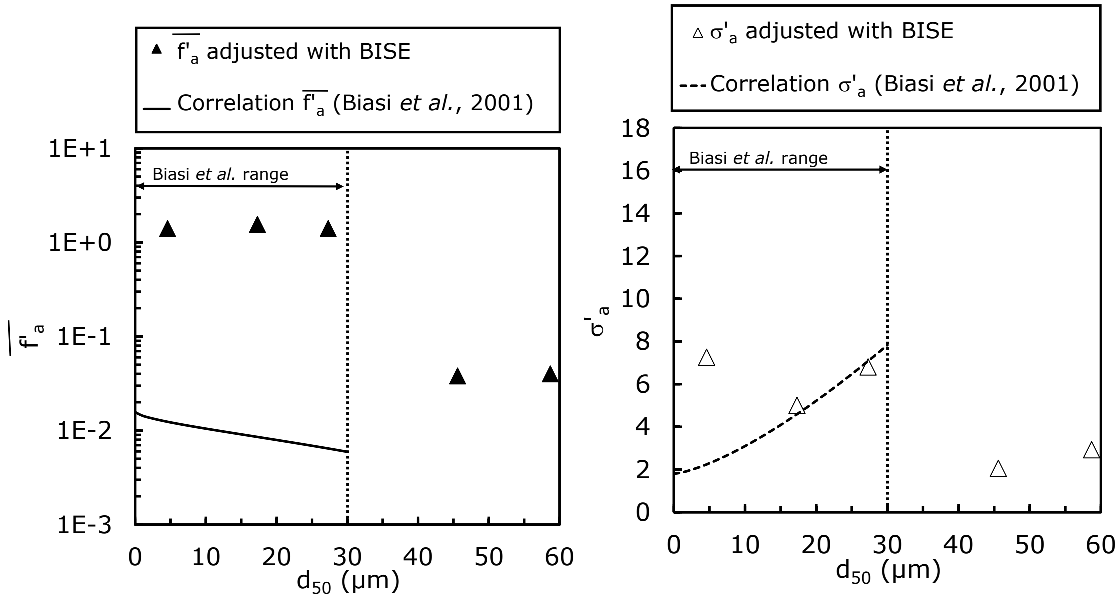

Figure 19 - Comparison of values $\overline{f'_a}$ and σ'_a fitted in BISE with the relationships $\overline{f'_a}$ and σ'_a of Biasi *et al.* (2001) as a function of the particle median diameter

The graphs in Figure 19 show that our values $\overline{f'_a}$ and σ'_a are relatively scattered. Because of this, fitting a model is not appropriate. It is not therefore possible for us to establish relationships which characterize the adhesion forces in the case of a pile of powder, which would permit the calculation of the resuspended fractions to validate the rock 'n' roll model using our data.

Besides, if we compare our fitted values $\overline{f'_a}$ to the relationship of Biasi *et al.* (2001), we find that our values $\overline{f'_a}$ are greater than unity in the range of validity of this model. However, the current knowledge of cohesion within a pile of powder does not allow to put forward satisfactory hypotheses for describing the changes in $\overline{f'_a}$ and σ'_a determined with BISE, as Biasi *et al.* (2001)do in their study.

5.3 Discussion

The comparison of our results with a macroscopic model (that of A. Fromentin) and a microphysical model (that of M.W. Reeks and D. Hall as modeled by L. Biasi *et al.*) from the literature emphasizes again the complexity of the resuspension phenomenon. The analyses show the limitations of current models' explanatory power.

In the Fromentin model, an essential input parameter was omitted, the particle size distribution. Therefore, since Fromentin's experimental conditions are no longer met, the model is no longer valid. For larger particle size distributions, the model seriously underestimates our experimental data. Additionally, this model does not predict resuspension once the friction velocity is less than 0.29 m/s (V = 5 m/s in BISE).

The Rock 'n roll model of Biasi *et al.* (2001), confirms many observations highlighted in our experiments, especially the influence of parameters such as exposure time and the shape of the deposit. Moreover, if the model of Biasi *et al.* (2001)did not fit our experimental results well, because of the variation of our phenomenon over six orders of magnitude, the approach of Biasi *et al.* (2001)for developing the relationships of $\overline{f'_a}$ and σ'_a as a function of the particle median diameter allows to obtains for each particle median diameter, a pair of values $\left(\overline{f'_a},\ \sigma'_a\right)$ which allows the fitting of the best rock 'n' roll model with our results. However, this approach does not allow to establish relationships for validating the Rock 'n roll model in our experimental conditions. This model does not apply in such a straightforward way to our data.

Faced with such results, it is therefore necessary for us to develop a novel semi-empirical relationship to describe resuspension caused by the air flowing over a powder deposit.

6 Research on a dimensionless model

The aim is to develop a model which combines experimental results with the physics of resuspension. This is why we speak of a *semi-empirical relationship.*

6.1 Procedure

In order to develop this model, we recall several key findings which emerged from our experimental study presented in Chapter 3:

- The friction velocity of the air v_* and the powder particle size distribution as described by its median diameter d_{50}, are the two basic parameters of resuspension. So they must appear in our relationship.
- The resuspension fraction K_R is an increasing function of v_* and d_{50} (see Figure 4).
- The resuspension fraction varies over several orders of magnitude in the experimental domain studied (10^{-6} to 1, see graphs in Figure 5.), which justifies, as we have done previously, using log K_R to analyze the data.

On the other hand, if we compare these results to the theories in the literature, we find that:

- Although our data derive from a macroscopic approach to the problem, it is possible to apply our results to a simple analysis of resuspension, using a balance of forces approach (Phillips, 1980). This allows us to confirm the presence of a threshold free-stream velocity which decreases as d_{50} increases in the particle size distribution range studied, but more importantly, it suggests that the changes in K_R can be correctly described by a power law in d_{50} and v_*.

- Finally, several dimensionless parameters are commonly used in the field of resuspension (Ziskind *et al.*, 1995),but the diameter d_p+ is of particular interest because it incorporates both the friction velocity of the air and the particle size distribution. Additionally, this dimensionless number reflects the interaction that is observed between these two parameters, as mediated by their product. Applied to the median diameters that characterize our powders, it becomes:

$$d_{50}+ \quad = \quad \frac{d_{50}.v_*}{\nu}. \tag{6.1}$$

As a result, all these data led to propose a relationship of the type:

$$\log K_R = a_0 + a_1 \log(d_{50}+). \tag{6.2}$$

This function can be obtained by linear regression on our experimental results after logarithmic transformations of K_R and d_{50}+. Therefore, this approach provides the relationship giving K_R as a function of d_{50} and v_* is of the form:

$$K_R \quad = \quad 10^{a_0}(d_{50}+)^{a_1}. \tag{6.3}$$

6.2 Proposed relationship and its range of validity

To stick with the results given in Chapter 3, the experiments that had been performed under the conditions described below were not used in the regression and hence in the model development. These consist of:

- Experiments on powders of a 5 micron median diameter. In fact, we saw that the resuspension obtained with these particles had to be attributable to the formation of larger agglomerates which are resuspended,
- Tests whose raw scores gave values of $K_R \leq \frac{LD_{SE}}{2}$ and which are below their threshold friction velocity. In fact, these values of K_R can be significantly smaller. Hence, their inclusion in the relationship might overestimate very low values of K_R.
- Experiments whose exposure time is less than 2 minutes. For exposure times less than this, we believe that our measurement method is not sufficiently reliable. On the other hand, we found that when very short exposure periods are combined with low accelerations, the transition phase is a significant proportion of the test duration and, because of this, may influence the value of K_R.

On the other hand, we noted that, between the stages of surface resuspension and deformation, resuspension is difficult to control, and a parameter which has little influence for very low or very high resuspension fractions may then play a significant role. This is the case for two secondary parameters brought to light in our experimental study, especially when their values are at the limits of their range of variation. Therefore, in this so-called transition zone, we also eliminate experiments with high accelerations and/or dry powders. From the union of the intervals described in Table 1, the latter is estimated to be $0.9 \leq d_{50}+ \leq 1.5$ throughout the BISE experimental domain.

Consequently, fitting 138 experimental resuspension fraction values allows to propose the following relationship:

$$K_R \quad = \quad 6{,}4.10^{-3}.(d_{50}+)^{5{,}7}\,. \qquad (6.4)$$

We compare this with our experimental data. Figure 20 shows the experimental resuspension fractions K_R as a function of those calculated using our semi-empirical relationship.

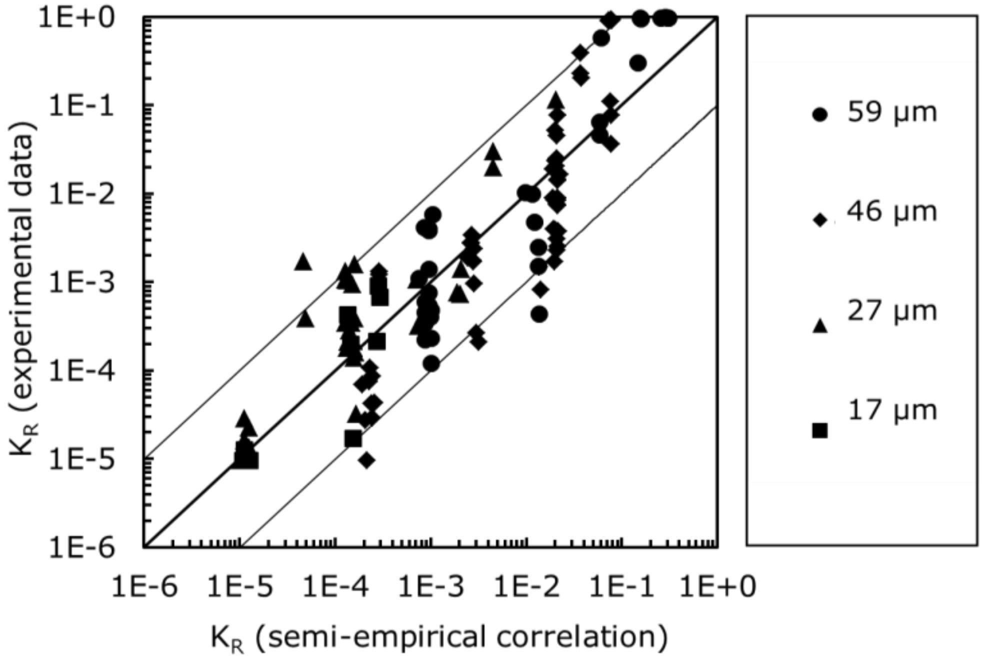

Figure 20 - Experimental resuspension fractions versus the fractions calculated from the semi-empirical relationship

The limits indicating ± an order of magnitude were defined in Report PSN-RES/SCA/LPMA/12-20 based on the analysis of all our results. Under these conditions, 90% of our data are included in this interval.

Given the variability of the phenomenon studied and the large range of variation in K_R (in our experiments, from 10^{-6} to 1), we can conclude that our model, although simple in its description, is quite satisfactory and represents our experimental results fairly well.

This semi-empirical relationship, a function of two primary resuspension parameters, is valid throughout the BISE experimental domain for:

- Al_2O_3 particles of size between 17 and 59 microns,
- air friction velocities between 0.07 and 0.52 m/s ($1 \leq V \leq 10$ m/s),
- exposure times ≥ 2 min.

However, in the transition zone at extreme values of the secondary parameters (water content and acceleration) our relationship does not hold.

Experiments performed under these conditions are shown in Figure 21. We can see there our estimated relationship ± an order of magnitude as a function of the dimensionless diameter as well as the experimental fractions measured for high accelerations (30 m/s^2) and/or dry powders in the transition zone.

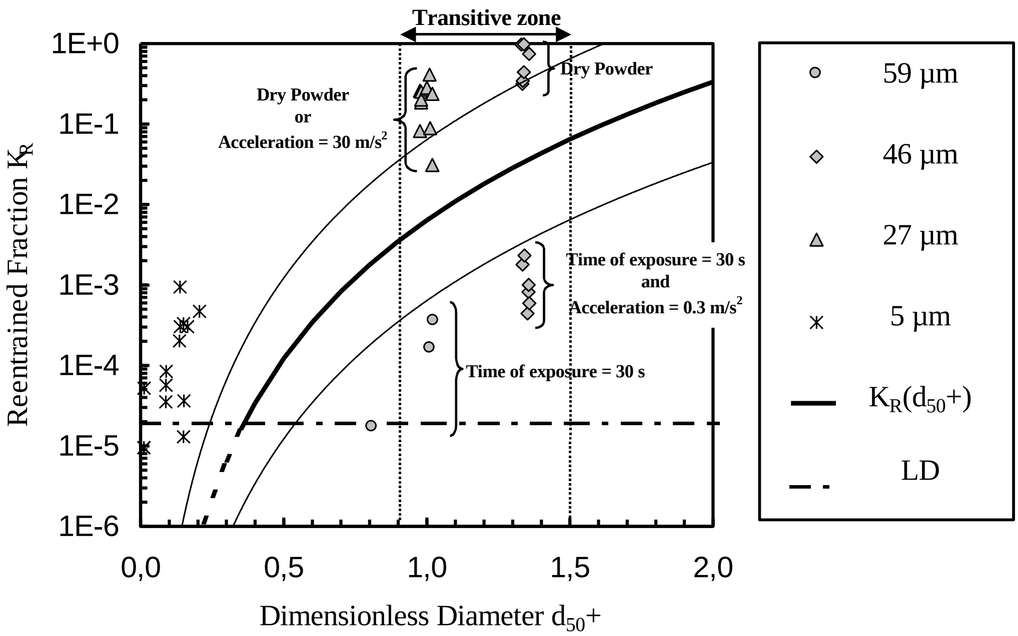

Figure 21 - Experimental resuspension fraction as a function of the dimensionless diameter for the limiting conditions of moisture content and acceleration, and for particle sizes of 5 microns and an exposure time of less than 2 min. Relationship $K_R(d_{50}+)$ following equation (6.4) and confidence interval to ± an order of magnitude

This graph shows that in the interval $0.9 \leq d_{50}+ \leq 1.5$, our relationship underestimates the experimental results for high accelerations and/or dry powders. In this field of study, our relationship is thus valid for limited ranges of the two secondary endpoints, namely:

$H_2O > 10$ mgH_2O/g.

and

$\alpha \leq 21$ m/s^2.

Here, we recall that the effect of acceleration is specific to our facility; this effect is related to exceeding the experimental free-stream velocity. Consequently, this restriction should not apply in general.

In addition, we introduce on the graph in Figure 21, the values of K_R obtained for exposure times less than 2 minutes and/or coupled with low accelerations, and for powders with a median diameter of 5 microns. For short durations (with or without low accelerations), we find that our data are not representative of the phenomenon because of our measurement technique. On the other hand, for powders of 5 microns, the relationship predicted that their resuspension should be lower than our measurements by at least two orders of magnitude, which is in good agreement with adhesion theory.

In conclusion, under an "envelope" approach to the resuspension fraction, the change in the resuspension fraction described in Figure 21 allows us to suggest that beyond $d_{50}+ \geq 0.9$, one should consider that resuspension is total, i.e., $K_R = 1$. Below this value, the relationship (6.4) correctly represents the resuspension by an air flow of a deposit of polydispersed powder.

7 Conclusion

Our comparison with recent models from the literature shows that in their present formulation, these models do not correctly describe the resuspension fractions in our experimental data. However, if one only considers the amount of material resuspended and not the actual size distributions of the resuspended particles (agglomeration phenomenon), our experimental data are consistent with the models of Fromentin (1989) and Biasi *et al.* (2001), only for 5 micron-sized particles.

To fill this gap, we have suggested a semi-empirical relationship. This relationship describes the fraction resuspended by an air flow over a pile of powder as a function of the dimensionless parameter $d_{50}+$. This dimensionless number incorporates the two primary parameters identified in our study, namely the friction velocity of the air and the particle size distribution of the powder. This relationship is written in the form:

$$K_R = 6{,}4.10^{-3}.(d_{50}+)^{5{,}7}$$

It is valid for $0.3 \leq d_{50}+ \leq 2.0$ in the BISE setup, namely:

- particle sizes of Al_2O_3: $17 \leq d_{50} \leq 59$ microns,
- friction velocities : $0.07 \leq v_* \leq 0.52$ m/s ($1 \leq V \leq 10$ m/s),
- exposure times: $\Delta t \geq 2$ min,
- moisture contents of the powder: $0 \leq H_2O \leq 1$ mgH_2O/g,
- accelerations: $0.3 \leq \alpha \leq 31$ m/s^2.

Nevertheless, in the region $0.9 \leq d_{50}+ \leq 1.5$, the secondary parameters are restricted to:

$H_2O > 0$ mgH_2O/g and $\alpha \leq 21$ m/s^2.

The confidence interval of this relationship is estimated to $\pm$ an order of magnitude.

The experimental design (Report WP2.3.3 D23.32) allowed, first, to highlight the most influential parameters. Thus, we have shown that the free-stream velocity and particle size distribution make a much more significant contribution than the other six factors; these two parameters play an important role in the resuspension. In addition, a strong positive interaction was observed between these two parameters. So, the effect of free-stream velocity on K_R differs depending on the powder particle size distribution. This allowed us to use alumina powders with the same particle size distribution as HTR graphite dust as a surrogate.

Moreover, the specific study of these two factors revealed that the resuspension process is a threshold phenomenon: there is a free-stream velocity threshold under which the resuspension fraction is below our detection limit. In our experiments, this free-stream velocity is higher when the particle size distribution of the powder in the heap is lower.

We have also been able to demonstrate the effect of so-called secondary parameters. Indeed, the moisture content of the powder has, as expected, a negative effect on resuspension. On the other hand, it is clear that the acceleration (for high values) plays a secondary role. However, we attribute this effect, not to the acceleration itself, but to the strong turbulence and high instantaneous velocities generated in our high acceleration tests.

We have also conducted specific studies on the exposure duration and the shape of the deposit. These show that most of the resuspension of the deposit occurs in the first few seconds. Thus, after a 15-minutes exposure period, the resuspension fraction tends to stabilize and becomes independent of time. Additionally, we found that the resuspension fraction does not depend on the shape of the heap. However, we found that, for free-stream velocity leading to high resuspension fraction values, the resuspension process depends mainly on the height of the deposit and the velocity gradient near the wall. However, given the strong influence of the primary and secondary parameters, these factors do not have a significant influence on resuspension. The same holds for the tap density of the powder and roughness of the test surface.

Photographic sequences describing the resuspension process in the BISE facility have confirmed that the resuspension of a conical deposit occurs in two concurrent phases. One is governed by a so-called "superficial" resuspension process which is analogous to multilayer deposition, and the other only begins above a speed which deforms a pile of powder. During this deformation stage two main resuspension processes which depend on the initial conditions, may be observed. Firstly, there is a localized phenomenon on the surface facing the air flow, wherein the resuspension is related to the free-stream velocity of the air directly incident on this surface. Secondly there is a phenomenon located downstream of the pile which is due to the presence of a recirculation zone (a phenomenon similar to that of a wake). But depending on the shapes of the deposit, these phenomena may change, making the physical description of resuspension very complex.

From all of our experimental results (a dataset of 227 experiments), we determined our experimental variability at the 95% confidence level. We measured this to ± one order of magnitude. We also showed that when the experimental resuspension fraction is greater than about 10^{-4}, less than 5% of the variability is attributable to our measurements. Under these conditions, the variability of the results largely arises from the phenomenon of resuspension.

Finally, we compared our data to two models found in the literature. This comparison showed that these resuspension models are not valid, in their current formulation, for a "pile" of powder whose particle size distribution has a median diameter greater than 5 microns. Thus, we proposed a semi-empirical relationship for calculating the resuspension fraction in our experimental conditions. This model, based on a dimensionless parameter that incorporates the two primary parameters of the resuspension process is valid throughout the BISE experimental domain, except in the resuspension transition zone, where the secondary parameters (moisture content and acceleration) vary on smaller scales.

Given the variability of the phenomenon studied and the large range of variation in K_R (in our experiments, from 10^{-6} to 1), we may conclude that our model, although simple in its description, is quite satisfactory and represents our experimental results well.

8 References

Alloul, L., (2002). Reentraînement par écoulement d'air d'une contamination particulaire déposée sur une surface. Thèse de doctorat de l'université Paris XII.

Andreotti, B., Claudin, P., Douady, S. (2002), Selection of dune shapes and velocities. Part 1 : Dynamics of sand, wind and barchans. *Cond-mat/0201103. Eur. Phys. J. B.*

Bagnold, R. A. (1941). The physics of blown sands and desert dunes. London: Methuen, 265p.

Biasi, L., De Los Reyes, A., Reeks, M. W., De Santi, G. F. (2001), Use of a simple model for the interpretation of experimental data on particle resuspension in turbulent flows. *J. Aerosol Sci.,***32,** 1175-1200.

Dauchot, O., Lechénault F., Gasquet, C. (2001), Barchan Dunes in the lab*. Cond-mat/0108378. Soumis aux Comptes Rendus de l'Académie des Sciences.*

Foucault, J. M. (1994),Etude théorique et expérimentale des phénomènes d'envol et de saltation de particules dans une couche limite turbulente. *Thèse de doctorat.* Université des Sciences et de Technologies de Lille, 6 octobre 1994.

Fromentin, A. (1989), Particle resuspension from a multi-layer deposit by turbulent flow. Doctoral thesis. Paul Scherrer Institute. **PSI-Bericht Nr. 38,** September 1989.

Gensdarmes F. and Roynette A. (2011), BISE Test Facility Description Report.WP2.3.3, D23.31..

Peillon S., Gensdarmes F. and Roynette A. (2012), BISE Test matrix Description Report.WP2.3.3, D23.32.

Phillips, M. (1980), A Force Balance Model for Particle Entrainment into a Fluid Stream*. J. Phys. D : Appl. Phys.,* **13**, 221-233.

Reeks, M. W., **Hall, D.** (2001), Kinetic models for particle suspension in turbulent flows: theory and measurement. *J. Aerosol Sci.,***32,** 1-31.

Ziskind, G., Fichman, M., Gutfinger, C. (1995), Resuspension of particulates from surfaces to turbulent flows - Review and analysis. *J. Aerosol Sci.*, **26,** 613-644.

9 Annexes

Annex 1 – Experimental results

9.1 Annex 1: Experimental results

The experimental results in the table below are arranged in ascending order of particle median diameter d_{50}, and then by free-stream velocity V.

We classify the experiments as follows:

If the experiment was conducted as part of an experimental design (For Example: *12.11p 1.2*):

1) The experimental design implemented *(12.11p ...)*
2) The experiment number in the design (*… 1…*)
3) The treatment repetition number (*… .2*)

If the experiment was not conducted as part of an experimental design (For Example: *d60-v1-mtas-t2-1)*:

1) The particle median diameter in the experiment *(d60 ...)*
2) The free-stream velocity in the experiment (*…v1…*)
3) Optionally, the type of the study (*…mtas-t2…*)
4) The treatment repetition number (*… .-1*)

Table 3 - Summary of BISE results

No.	Experiment	d_{50}	Pile shape	ρ_{pile}	H_2O	Rug_{SE}	V	Δt	α	K_R
1	*12.11p 5.1*	4.6	Cone H,d	1.5	1.3	1.6	0.5	60.0	2.2	**$9.5\times10^{-6*}$**
2	*12.11p 11.1*	4.6	Cone H,d	1.7	1.3	0	0.5	2.0	2.0	**$9.5\times10^{-6*}$**
3	*12.11p 1.2*	4.6	Cone h,D	1.5	0.0	0	0.5	2.0	0.4	**5.2×10^{-5}**
4	*d5-v5-1*	4.6	Cone H,d	1.7	1.3	1.6	5.1	15.0	1.5	**3.5×10^{-5}**
5	*d5-v5-2*	4.6	Cone H,d	1.7	1.3	1.6	5.1	15.0	1.5	**5.7×10^{-5}**
6	*13.2p 5.2*	4.6	Cone H,d	1.7	1.3	1.6	5.2	15.0	1.5	**8.5×10^{-5}**
7	*d5-v8,5-2*	4.6	Cone H,d	1.7	1.3	1.6	8.4	15.0	1.5	**2.0×10^{-4}**
8	*d5-v8,5-1*	4.6	Cone H,d	1.8	1.3	1.6	8.6	15.0	1.5	**9.4×10^{-4}**
9	*d5-v8,5-3*	4.6	Cone H,d	1.7	1.3	1.6	8.6	15.0	1.5	**3.0×10^{-4}**
10	*12.11p 6.2*	4.6	Cone h,D	1.7	0.0	1.6	9.4	2.0	2.3	**$1.3\times10^{-5**}$**
11	*12.11p 3.1*	4.6	Cone H,d	1.8	0.0	1.6	9.5	60.0	0.5	**3.3×10^{-4}**
12	*12.11p 7.1*	4.6	Cone H,d	1.5	1.3	0	9.5	60.0	0.5	**3.6×10^{-5}**
13	*d5-v10-1*	4.6	Cone H,d	1.7	1.3	1.6	10.5	15.0	1.6	**3.0×10^{-4}**
14	*d5-v13,5-1*	4.6	Cone H,d	1.4	1.3	1.6	13.6	15.0	1.5	**4.7×10^{-4}**
15	*13.2p 1.2*	17.3	Cone H,d	1.8	0.8	1.6	2.0	15.0	1.5	**9.5×10^{-6}**
16	*13.2p 1.1*	17.3	Cone H,d	1.8	0.8	1.6	2.0	15.0	1.5	**$9.5\times10^{-6*}$**
17	*d16-v5-2*	17.3	Cone H,d	1.8	0.8	1.6	5.0	15.0	1.5	**9.5×10^{-6}**
18	*d16-v5-1*	17.3	Cone H,d	1.7	0.8	1.6	5.1	15.0	1.5	**$1.3\times10^{-5**}$**
19	*d16-v5-3*	17.3	Cone H,d	1.7	0.8	1.6	5.2	15.0	1.5	**9.5×10^{-6}**
20	*13.2p 3.1*	17.3	Cone H,d	1.7	0.8	1.6	8.4	15.0	1.4	**4.2×10^{-4}**
21	*d16-v8,5-2*	17.3	Cone H,d	1.7	0.8	1.6	8.5	15.0	1.5	**2.0×10^{-4}**
22	*d16-v8,5-1*	17.3	Cone H,d	1.8	0.8	1.6	8.6	15.3	1.5	**$1.7\times10^{-5**}$**
23	*d16-v10-2*	17.3	Cone H,d	1.7	0.8	1.6	9.7	15.0	1.5	**2.1×10^{-4}**
24	*d16-v10-3*	17.3	Cone H,d	1.7	0.8	1.6	9.7	15.0	1.5	**9.1×10^{-4}**
25	*d16-v10-1*	17.3	Cone H,d	1.8	0.8	1.6	9.8	15.0	1.5	**6.7×10^{-4}**
26	*13.2p 7.1*	27.3	Cone H,d	1.7	0.8	1.6	0.5	15.0	1.5	**9.5×10^{-6}**
27	*d30-v3-1*	27.3	Cone H,d	1.7	0.8	1.6	2.9	15.0	1.5	**9.5×10^{-6}**
28	*d30-v3-mtas-t0,5-2*	27.3	Cone H,d	1.7	0.8	1.6	3.0	0.5	1.5	**9.5×10^{-6}**
29	*d30-v3-mtas-t2-2*	27.3	Cone H,d	1.7	0.8	1.6	3.0	2.0	1.5	**9.5×10^{-6}**
30	*d30-v3-mtas-t15-2*	27.3	Cone H,d	1.7	0.8	1.6	3.0	15.0	1.5	**$1.6\times10^{-5**}$**

* Measured $K_R \leq \frac{LD_{SE}}{2}$ (it is attributed the value $\frac{LD_{SE}}{2}$)

** $\frac{LD_{SE}}{2} < K_R \leq LD_{SE}$

No.	Experiment	d_{50}	Pile shape	ρ_{pile}	H_2O	Rug_{SE}	V	Δt	α	K_R
31	*d30-v3-mtas-t30-2*	27.3	Cone H,d	1.7	0.8	1.6	3.0	30.0	1.5	**$1.5\times10^{-5**}$**
32	*d30-v3-mtas-t60-2*	27.3	Cone H,d	1.7	0.8	1.6	3.0	60.0	1.5	**2.9×10^{-5}**
33	*d30-v3-mtas-t0,5-1*	27.3	Cone H,d	1.8	0.8	1.6	3.1	0.5	1.5	**9.5×10^{-6}**
34	*d30-v3-mtas-t2-1*	27.3	Cone H,d	1.8	0.8	1.6	3.1	2.0	1.5	**9.5×10^{-6}**
35	*d30-v3-mtas-t15-1*	27.3	Cone H,d	1.8	0.8	1.6	3.1	15.0	1.5	**$1.3\times10^{-5**}$**
36	*d30-v3-mtas-t30-1*	27.3	Cone H,d	1.8	0.8	1.6	3.1	30.0	1.5	**$1.2\times10^{-5**}$**
37	*d30-v3-mtas-t60-1*	27.3	Cone H,d	1.8	0.8	1.6	3.1	60.0	1.5	**2.3×10^{-5}**
38	*16.4p - 3.1*	27.3	Cone H,d	1.8	0.8	0	4.0	60.0	14.3	**1.7×10^{-3}**
39	*16.4p - 5.1*	27.3	Cone H,d	1.8	0.0	12.5	4.1	60.0	0.5	**3.9×10^{-4}**
40	*16.4p - 1.1*	27.3	Cone H,d	1.7	0.0	0	4.1	0.5	0.5	**8.2×10^{-4}**
41	*16.4p - 7.1*	27.3	Cone H,d	1.8	0.8	12.5	4.1	0.5	14.2	**7.5×10^{-4}**
42	*d30-v5-2-t30*	27.3	Cone H,d	1.7	0.8	1.6	4.9	30.0	1.5	**1.3×10^{-3}**
43	*12.11p 13.1*	27.3	Cone H,d	1.7	0.8	1.6	4.9	15.0	1.4	**1.1×10^{-3}**
44	*12.11p 13.2*	27.3	Cone H,d	1.7	0.8	1.6	4.9	15.0	1.4	**3.4×10^{-4}**
45	*12.11p 13.4*	27.3	Cone H,d	1.7	0.8	1.6	5.0	15.0	1.2	**1.0×10^{-3}**
46	*12.11p 13.5*	27.3	Cone H,d	1.7	0.8	1.6	5.0	15.0	1.2	**1.8×10^{-4}**
47	*12.11p 13.8*	27.3	Cone H,d	1.8	0.8	1.6	5.0	15.0	1.2	**2.1×10^{-4}**
48	*12.11p 13.9*	27.3	Cone H,d	1.7	0.8	1.6	5.0	15.0	1.0	**3.6×10^{-4}**
49	*13.2p d30-v5-t15-1*	27.3	Cone H,d	1.8	0.8	1.6	5.0	15.0	1.5	**4.2×10^{-4}**
50	*12.11p 13.6*	27.3	Cone H,d	1.7	0.8	1.6	5.0	15.0	1.3	**2.8×10^{-4}**
51	*12.11p 13.7*	27.3	Cone H,d	1.8	0.8	1.6	5.1	15.0	1.2	**3.4×10^{-4}**
52	*12.11p 13.11*	27.3	Cone H,d	1.8	0.8	1.6	5.1	15.0	1.0	**9.4×10^{-4}**
53	*13.2p 9.3*	27.3	Cone H,d	1.7	0.8	1.6	5.1	15.0	1.5	**2.1×10^{-4}**
54	*d30-v5-t2-1*	27.3	Cone H,d	1.8	0.8	1.6	5.1	2.0	1.5	**1.4×10^{-4}**
55	*13.2p d30-v5-t15-2*	27.3	Cone H,d	1.8	0.8	1.6	5.1	15.0	1.5	**1.8×10^{-4}**
56	*12.11p 13.10*	27.3	Cone H,d	1.7	0.8	1.6	5.1	15.0	1.0	**1.6×10^{-3}**
57	*13.2p 9.4*	27.3	Cone H,d	1.7	0.8	1.6	5.2	15.0	1.5	**3.9×10^{-4}**
58	*13.2p 9.2*	27.3	Cone H,d	1.8	0.8	1.6	5.2	15.0	1.5	**1.6×10^{-4}**
59	*13.2p 9.1*	27.3	Cone H,d	1.8	0.8	1.6	5.2	15.0	1.6	**3.2×10^{-5}**
60	*d30-v7-2*	27.3	Cone H,d	1.8	0.8	1.6	6.9	15.0	1.5	**1.1×10^{-3}**
61	*d30-v7-1*	27.3	Cone H,d	1.8	0.8	1.6	7.0	15.0	1.5	**3.1×10^{-4}**
62	*d30-v8,5-3*	27.3	Cone H,d	1.8	0.8	1.6	8.5	15.0	1.5	**7.6×10^{-4}**
63	*d30-v8,5-2*	27.3	Cone H,d	1.7	0.8	1.6	8.6	15.0	1.5	**7.2×10^{-4}**
64	*d30-v8,5-1*	27.3	Cone H,d	1.7	0.8	1.6	8.6	15.0	1.5	**1.4×10^{-3}**
65	*difftas-03-1*	27.3	Cone H,d	1.7	0.8	1.6	9.5	2.0	28.9	**8.2×10^{-2}**
66	*difftas-03-2*	27.3	Cone H,d	1.8	0.8	1.6	9.5	15.0	28.9	**2.6×10^{-1}**
67	*difftas-4-1*	27.3	Cone H,d	1.7	0.8	1.6	9.5	30.0	29.4	**2.5×10^{-1}**
68	*difftas-4-2*	27.3	Cone H,d	1.8	0.8	1.6	9.5	60.0	29.4	**1.9×10^{-1}**
69	*difftas-4-2'*	27.3	Cone H,d	1.7	0.8	1.6	9.5	60.0	29.4	**2.0×10^{-1}**
70	*mêmetas-t2-03*	27.3	Cone H,d	1.7	0.8	1.6	9.5	2.0	32.2	**3.0×10^{-2}**
71	*mêmetas-t15-03*	27.3	Cone H,d	1.7	0.8	1.6	9.5	15.0	32.2	**2.2×10^{-1}**
72	*mêmetas-t30-03*	27.3	Cone H,d	1.7	0.8	1.6	9.5	30.0	32.2	**2.9×10^{-1}**
73	*mêmetas-t60-03*	27.3	Cone H,d	1.7	0.8	1.6	9.5	60.0	32.2	**3.3×10^{-1}**
74	*mêmetas-t2-02*	27.3	Cone H,d	1.8	0.8	1.6	9.6	2.0	28.2	**4.3×10^{-2}**
75	*mêmetas-t15-02*	27.3	Cone H,d	1.8	0.8	1.6	9.6	15.0	28.2	**2.1×10^{-1}**
76	*mêmetas-t30-02*	27.3	Cone H,d	1.8	0.8	1.6	9.6	30.0	28.2	**2.7×10^{-1}**
77	*mêmetas-t60-02*	27.3	Cone H,d	1.8	0.8	1.6	9.6	60.0	28.2	**3.2×10^{-1}**
78	*mêmetas-t15-0*	27.3	Cone H,d	1.7	0.8	1.6	9.8	2.0	31.7	**1.1×10^{-2}**
79	*mêmetas-t30-01*	27.3	Cone H,d	1.7	0.8	1.6	9.8	15.0	31.7	**1.9×10^{-1}**
80	*mêmetas-t30-01*	27.3	Cone H,d	1.7	0.8	1.6	9.8	30.0	31.7	**2.6×10^{-1}**
81	*mêmetas-t60-0*	27.3	Cone H,d	1.7	0.8	1.6	9.8	60.0	31.7	**3.1×10^{-1}**
82	*difftas-02-1*	27.3	Cone H,d	1.8	0.8	1.6	9.8	30.0	33.7	**2.7×10^{-1}**
83	*difftas-02-2*	27.3	Cone H,d	1.7	0.8	1.6	9.8	60.0	33.7	**2.8×10^{-1}**
84	*16.4p - 13.1*	27.3	Cone H,d	1.8	0.0	12.5	9.9	60.0	14.3	**4.1×10^{-1}**
85	*16.4p - 9.1*	27.3	Cone H,d	1.7	0.0	0	9.9	0.5	14.5	**8.9×10^{-2}**
86	*16.4p - 15.1*	27.3	Cone H,d	1.8	0.8	12.5	9.9	0.5	0.5	**1.7×10^{-2}**
87	*difftas-01-1*	27.3	Cone H,d	1.7	0.8	1.6	10.0	2.0	31.4	**3.1×10^{-2}**
88	*difftas-01-2*	27.3	Cone H,d	1.7	0.8	1.6	10.0	15.0	31.4	**2.4×10^{-1}**
89	*13.2p 8.1*	27.3	Cone H,d	1.8	0.8	1.6	10.1	15.0	1.6	**2.0×10^{-2}**
90	*13.2p 8.2*	27.3	Cone H,d	1.7	0.8	1.6	10.1	15.0	1.6	**3.0×10^{-2}**
91	*d30-v13,5-1*	27.3	Cone H,d	1.8	0.8	1.6	13.7	15.0	1.5	**1.2×10^{-1}**

No.	Experiment	d_{50}	Pile shape	ρ_{pile}	H_2O	Rug_{SE}	V	Δt	α	K_R
92	13.2p 2.1	45.6	Cone H,d	1.7	1.0	1.6	2.0	15.0	1.5	**$9.5\times10^{-6*}$**
93	d45-v2- Gal-1	45.6	Disc	1.8	1.0	1.6	2.0	15.0	1.5	**9.5×10^{-6}**
94	d45-v3-1-Obél	45.6	Truncated pyramid	1.8	1.0	1.6	3.0	15.0	1.5	**6.9×10^{-5}**
95	d45-v3-3	45.6	Cone H,d	1.7	1.0	1.6	3.0	15.0	1.5	**2.7×10^{-5}**
96	d45-v3-Gal-2	45.6	Disc	1.8	1.0	1.6	3.0	15.0	1.6	**9.5×10^{-6}**
97	d45-v3-Gal-3	45.6	Disc	1.7	1.0	1.6	3.1	15.0	1.5	**7.5×10^{-5}**
98	d45-v3-Obél-2	45.6	Truncated pyramid	1.8	1.0	1.6	3.1	15.0	1.5	**1.1×10^{-4}**
99	d45-v3-Gal 4	45.6	Disc	1.7	1.0	1.6	3.1	15.0	1.5	**4.2×10^{-5}**
100	d45-v3-1	45.6	Cone H,d	1.8	1.0	1.6	3.1	15.0	1.5	**8.5×10^{-5}**
101	d45-v3- Obél-3	45.6	Truncated pyramid	1.8	1.0	1.6	3.1	15.0	1.5	**2.9×10^{-5}**
102	d45-v3-2	45.6	Cone H,d	1.8	1.0	1.6	3.1	15.0	1.7	**4.3×10^{-5}**
103	d45-v3-ssH2O-1	45.6	Cone H,d	1.8	0.0	1.6	3.2	15.0	1.3	**1.3×10^{-3}**
104	d45-v3-ssH2O-2	45.6	Cone H,d	1.7	0.0	1.6	3.2	15.0	1.6	**1.2×10^{-3}**
105	d45-v5-5	45.6	Cone H,d	1.7	1.0	1.6	5.0	15.0	1.5	**1.9×10^{-3}**
106	d45-v5-Gal-2	45.6	Disc	1.8	1.0	1.6	5.0	15.0	1.5	**2.8×10^{-3}**
107	d45-v5-Obél-1	45.6	Truncated pyramid	1.8	1.0	1.6	5.0	15.0	1.6	**2.7×10^{-3}**
108	d45-v5-Gal-1	45.6	Disc	1.7	1.0	1.6	5.0	15.0	1.6	**3.4×10^{-3}**
109	d45-v5-Obé-3	45.6	Truncated pyramid	1.7	1.0	1.6	5.1	15.0	1.6	**1.8×10^{-3}**
110	d45-v5-Gal-3	45.6	Disc	1.7	1.0	1.6	5.1	15.0	1.5	**1.7×10^{-3}**
111	d45-v5-2	45.6	Cone H,d	1.8	1.0	1.6	5.1	15.0	1.4	**9.5×10^{-4}**
112	d45-v5-Obél-2	45.6	Truncated pyramid	1.7	1.0	1.6	5.1	15.0	1.6	**2.4×10^{-3}**
113	d45-v5-1	45.6	Cone H,d	1.8	1.0	1.6	5.1	15.0	1.5	**2.6×10^{-4}**
114	d45-v5-3	45.6	Cone H,d	1.8	1.0	1.6	5.2	15.0	1.5	**2.1×10^{-4}**
115	16.4p - 18.1	45.6	Cone H,d	1.7	0.0	6.5	7.0	15.5	6.8	**3.1×10^{-3}**
116	16.4p - 20.1	45.6	Cone H,d	1.8	1.0	6.5	7.0	15.0	6.7	**1.5×10^{-3}**
117	16.4p - 19.1	45.6	Cone H,d	1.8	1.0	6.5	7.0	15.0	7.0	**8.2×10^{-4}**
118	16.4p - 17.1	45.6	Cone H,d	1.8	0.0	6.5	7.1	15.0	7.0	**1.3×10^{-2}**
119	8.3p 8.3	45.6	Cone H,d	1.8	1.0	12.5	7.5	60.0	20.4	**1.9×10^{-2}**
120	2.2p 1.2	45.6	Cone H,d	1.5	0.0	1.6	7.5	15.0	1.5	**9.7×10^{-1}**
121	2.2p 4.3	45.6	Cone H,d	2.0	1.0	1.6	7.5	15.0	1.5	**9.0×10^{-3}**
122	2.2p 3.3	45.6	Cone H,d	2.0	0.0	1.6	7.5	15.0	1.5	**3.2×10^{-1}**
123	2.2p 4.2	45.6	Cone H,d	2.0	1.0	1.6	7.5	15.0	1.5	**4.0×10^{-3}**
124	8.3p 5.1	45.6	Cone H,d	1.7	1.0	12.5	7.5	0.5	0.3	**1.8×10^{-3}**
125	2.2p 3.2	45.6	Cone H,d	2.0	0.0	1.6	7.5	15.0	1.5	**3.5×10^{-1}**
126	8.3p 2.3	45.6	Cone H,d	1.8	1.0	0	7.5	0.5	19.7	**2.5×10^{-3}**
127	2.2p 2.3	45.6	Cone H,d	1.5	1.0	1.6	7.5	15.3	1.5	**1.7×10^{-3}**
128	d45-v7,5-Obél-3	45.6	Truncated pyramid	1.8	1.0	1.6	7.5	15.0	1.5	**8.4×10^{-3}**
129	2.2p 3.1	45.6	Cone H,d	2.0	0.0	1.6	7.5	15.0	1.5	**9.8×10^{-1}**
130	2.2p 1.3	45.6	Cone H,d	1.5	0.0	1.6	7.5	15.0	1.5	**4.4×10^{-1}**
131	d45-v7,5-Gal-1	45.6	Disc	1.7	1.0	1.6	7.5	15.0	1.6	**2.4×10^{-2}**
132	8.3p 1.1	45.6	Cone H,d	1.7	1.0	0	7.5	0.5	0.3	**2.3×10^{-3}**
133	2.2p 2.2	45.6	Cone H,d	1.5	1.0	1.6	7.5	15.0	1.5	**3.9×10^{-3}**
134	8.3p 3.3	45.6	Cone H,d	1.7	1.0	0	7.5	60.3	0.3	**5.2×10^{-2}**
135	8.3p 2.1	45.6	Cone H,d	1.8	1.0	0	7.6	0.5	20.5	**5.1×10^{-3}**
136	8.3p 6.1	45.6	Cone H,d	1.7	1.0	12.5	7.6	0.5	21.4	**1.0×10^{-2}**
137	d45-v7,5-Gal-2	45.6	Disc	1.8	1.0	1.6	7.6	15.0	1.4	**2.0×10^{-2}**
138	-d45-v7,5-Gal 3	45.6	Disc	1.8	1.0	1.6	7.6	15.0	1.4	**4.5×10^{-2}**
139	8.3p 3.1	45.6	Cone H,d	1.7	1.0	0	7.6	60.0	0.3	**7.6×10^{-3}**
140	8.3p 4.2	45.6	Cone H,d	1.8	1.0	0	7.6	60.0	21.4	**1.0×10^{-1}**
141	8.3p 3.6	45.6	Cone H,d	1.8	1.0	0	7.6	60.0	0.3	**2.3×10^{-3}**

* Measured $K_R \leq \frac{LD_{SE}}{2}$ (it is attributed the value $\frac{LD_{SE}}{2}$)

No.	Experiment	d_{50}	Pile shape	ρ_{pile}	H_2O	Rug_{SE}	V	Δt	α	K_R
142	*8.3p 4.1*	45.6	Cone H,d	1.7	1.0	0	7.6	60.0	20.6	**2.5×10^{-2}**
143	*8.3p 6.2*	45.6	Cone H,d	1.7	1.0	12.5	7.6	0.5	20.6	**1.2×10^{-2}**
144	*8.3p 6.3*	45.6	Cone H,d	1.7	1.0	12.5	7.6	0.5	20.0	**1.4×10^{-2}**
145	*8.3p 5.3*	45.6	Cone H,d	1.8	1.0	12.5	7.6	0.5	0.3	**4.4×10^{-4}**
146	*8.3p 7.3*	45.6	Cone H,d	1.8	1.0	12.5	7.6	60.0	0.3	**3.1×10^{-3}**
147	*8.3p 7.2*	45.6	Cone H,d	1.8	1.0	12.5	7.6	60.0	0.3	**3.7×10^{-3}**
148	*d45-v7,5-Obél-2*	45.6	Truncated pyramid	1.8	1.0	1.6	7.6	15.0	1.5	**8.9×10^{-3}**
149	*d45-v7,5-Obél-1*	45.6	Truncated pyramid	1.8	1.0	1.6	7.6	15.0	1.5	**7.3×10^{-3}**
150	*8.3p 7.1*	45.6	Cone H,d	1.7	1.0	12.5	7.6	60.0	0.3	**1.4×10^{-2}**
151	*8.3p 1.2*	45.6	Cone H,d	1.8	1.0	0	7.6	0.5	0.3	**8.2×10^{-4}**
152	*8.3p 2.2*	45.6	Cone H,d	1.8	1.0	0	7.6	0.5	21.5	**1.5×10^{-2}**
153	*2.2p 2.1*	45.6	Cone H,d	1.5	1.0	1.6	7.6	15.0	1.5	**2.5×10^{-3}**
154	*8.3p 1.3*	45.6	Cone H,d	1.8	1.0	0	7.6	0.5	0.3	**1.0×10^{-3}**
155	*8.3p 8.1*	45.6	Cone H,d	1.7	1.0	12.5	7.6	60.0	20.8	**7.7×10^{-2}**
156	*8.3p 8.2*	45.6	Cone H,d	1.7	1.0	12.5	7.6	60.0	20.1	**1.4×10^{-2}**
157	*8.3p 3.2*	45.6	Cone H,d	1.7	1.0	0	7.6	60.0	0.3	**8.5×10^{-3}**
158	*2.2p 1.1*	45.6	Cone H,d	1.5	0.0	1.6	7.6	15.0	1.5	**7.4×10^{-1}**
159	*8.3p 5.2*	45.6	Cone H,d	1.8	1.0	12.5	7.7	0.5	0.3	**5.9×10^{-4}**
160	*2.2p 4.1*	45.6	Cone H,d	2.1	1.0	1.6	7.7	15.0	1.5	**3.7×10^{-3}**
161	*8.3p 4.3*	45.6	Cone H,d	1.8	1.0	0	7.7	60.0	20.3	**1.7×10^{-2}**
162	*13.2p 4.1*	45.6	Cone H,d	1.7	1.0	1.6	8.5	15.0	1.5	**3.9×10^{-1}**
163	*d45-v8,5-1*	45.6	Cone H,d	1.8	1.0	1.6	8.5	15.0	1.5	**2.3×10^{-1}**
164	*d45-v8,5-2*	45.6	Cone H,d	1.8	1.0	1.6	8.6	15.0	1.5	**2.0×10^{-1}**
165	*d45-v10-3*	45.6	Cone H,d	1.8	1.0	1.6	9.8	15.0	1.5	**9.1×10^{-1}**
166	*d45-v10-2*	45.6	Cone H,d	1.7	1.0	1.6	9.8	15.0	1.5	**9.0×10^{-1}**
167	*d45-v10-Gal-1*	45.6	Disc	1.7	1.0	1.6	9.9	15.0	1.5	**1.1×10^{-1}**
168	*d45-v10-Gal-3*	45.6	Disc	1.7	1.0	1.6	9.9	15.0	1.4	**3.7×10^{-2}**
169	*d45-v10-Obél-4*	45.6	Truncated pyramid	1.8	1.0	1.6	9.9	15.0	1.4	**9.2×10^{-1}**
170	*d45-v10-Obél-1*	45.6	Truncated pyramid	1.8	1.0	1.6	9.9	15.0	1.5	**7.7×10^{-2}**
171	*d45-v10-1*	45.6	Cone H,d	1.8	1.0	1.6	9.9	15.0	1.5	**9.0×10^{-1}**
172	*d45-v10-Obél-2*	45.6	Truncated pyramid	1.8	1.0	1.6	9.9	15.0	1.5	**9.0×10^{-1}**
173	*d45-v10-Gal-2*	45.6	Disc	1.8	1.0	1.6	10.0	15.0	1.5	**7.4×10^{-2}**
174	*12.11p 12.1*	58.7	Cone h,D	2.0	1.1	1.6	0.5	2.0	0.5	**$9.5\times10^{-6*}$**
175	*12.11p 8.1*	58.7	Cone h,D	1.5	0.0	1.6	0.5	60.0	2.3	**9.5×10^{-6}**
176	*12.11p 10.1*	58.7	Cone H,d	2.0	0.0	0	0.5	60.0	0.5	**9.5×10^{-6}**
177	*d60-v1-mtas-t2-1*	58.7	Cone H,d	1.8	1.1	1.6	1.1	2.0	1.5	**9.5×10^{-6}**
178	*d60-v1-mtas-t15-1*	58.7	Cone H,d	1.8	1.1	1.6	1.1	15.0	1.5	**9.5×10^{-6}**
179	*d60-v1-mtas-t30-1*	58.7	Cone H,d	1.8	1.1	1.6	1.1	30.0	1.5	**9.5×10^{-6}**
180	*d60-v1-mtas-t60-1*	58.7	Cone H,d	1.8	1.1	1.6	1.1	60.0	1.5	**9.5×10^{-6}**
181	*d60-v1-mtas-t120-1*	58.7	Cone H,d	1.8	1.1	1.6	1.1	120.0	1.5	**9.5×10^{-6}**
182	*d60-v1-mtas-t17h-1*	58.7	Cone H,d	1.8	1.1	1.6	1.1	1020.0	1.5	**9.5×10^{-6}**
183	*d60-v3-4*	58.7	Cone H,d	1.8	1.1	1.6	2.9	15.0	1.5	**1.1×10^{-3}**
184	*d60-v3-5*	58.7	Cone H,d	1.7	1.1	1.6	3.0	15.0	1.5	**4.2×10^{-3}**
185	*d60-v3-mtas-t0,5-2*	58.7	Cone H,d	1.7	1.1	1.6	3.0	0.5	1.5	**2.0×10^{-4}**
186	*d60-v3-mtas-t2-2*	58.7	Cone H,d	1.7	1.1	1.6	3.0	2.0	1.5	**2.2×10^{-4}**
187	*d60-v3-mtas-t17-2*	58.7	Cone H,d	1.7	1.1	1.6	3.0	17.0	1.5	**3.4×10^{-4}**
188	*d60-v3-mtas-t30-2*	58.7	Cone H,d	1.7	1.1	1.6	3.0	30.0	1.5	**4.5×10^{-4}**
189	*d60-v3-mtas-t60-2*	58.7	Cone H,d	1.7	1.1	1.6	3.0	60.0	1.5	**5.9×10^{-4}**
190	*d60-v3-mtas-t0,5-3*	58.7	Cone H,d	1.8	1.1	1.6	3.1	0.5	1.5	**5.0×10^{-4}**
191	*d60-v3-mtas-t2-3*	58.7	Cone H,d	1.8	1.1	1.6	3.1	2.0	1.5	**5.4×10^{-4}**
192	*d60-v3-mtas-t15-3*	58.7	Cone H,d	1.8	1.1	1.6	3.1	15.0	1.5	**7.5×10^{-4}**
193	*d60-v3-mtas-t30-3*	58.7	Cone H,d	1.8	1.1	1.6	3.1	30.0	1.5	**1.4×10^{-3}**
194	*d60-v3-mtas-t60-3*	58.7	Cone H,d	1.8	1.1	1.6	3.1	60.0	1.5	**3.8×10^{-3}**

* Measured $K_R \leq \frac{LD_{SE}}{2}$ (it is attributed the value $\frac{LD_{SE}}{2}$)

No.	Experiment	d_{50}	Pile shape	ρ_{pile}	H_2O	Rug_{SE}	V	Δt	α	K_R
195	*d60-v3-2*	58.7	Cone H,d	1.8	1.1	1.6	3.1	15.0	1.5	**4.0×10^{-3}**
196	*d60-v3-t15-0*	58.7	Cone H,d	1.8	1.1	1.6	3.1	15.0	1.5	**4.0×10^{-4}**
197	*d60-v3-mtas-t1,5-1'*	58.7	Cone H,d	1.7	1.1	1.6	3.1	1.5	1.5	**2.2×10^{-5}**
198	*d60-v3-mtas-t15-1'*	58.7	Cone H,d	1.7	1.1	1.6	3.1	15.0	1.5	**1.2×10^{-4}**
199	*d60-v3-mtas-t30-1'*	58.7	Cone H,d	1.7	1.1	1.6	3.1	30.0	1.5	**2.3×10^{-4}**
200	*d60-v3-mtas-t60-1'*	58.7	Cone H,d	1.7	1.1	1.6	3.1	60.0	1.5	**4.7×10^{-4}**
201	*d60-v3-mtas-t0,5-1'*	58.7	Cone H,d	1.7	1.1	1.6	3.1	0.5	1.5	**$1.7\times10^{-5**}$**
202	*d60-v3-3*	58.7	Cone H,d	1.7	1.1	1.6	3.1	15.0	1.5	**5.8×10^{-3}**
203	*16.4p - 6.1*	58.7	Cone H,d	1.8	0.0	12.5	4.0	0.5	14.3	**1.6×10^{-4}**
204	*16.4p - 4.1*	58.7	Cone H,d	1.8	1.1	0	4.1	0.5	0.5	**3.6×10^{-4}**
205	*16.4p - 6.2'*	58.7	Cone H,d	1.9	0.0	1.6	4.1	0.5	15.0	**1.8×10^{-2}**
206	*16.4p - 6.3'*	58.7	Cone H,d	1.9	0.0	1.6	4.1	0.5	15.0	**3.3×10^{-2}**
207	*16.4p - 2.1*	58.7	Cone H,d	1.7	0.0	0	4.2	60.0	14.3	**4.6×10^{-3}**
208	*d60-v5-t15-1*	58.7	Cone H,d	1.7	1.1	1.6	4.9	15.0	1.4	**1.0×10^{-2}**
209	*d60-v5-2*	58.7	Cone H,d	1.7	1.1	1.6	5.1	15.0	1.5	**9.8×10^{-3}**
210	*d60-v5-1*	58.7	Cone H,d	1.7	1.1	1.6	5.1	15.0	1.5	**4.8×10^{-3}**
211	*13.2p 6.2*	58.7	Cone H,d	1.7	1.1	1.6	5.2	15.0	1.4	**1.5×10^{-3}**
212	*13.2p 6.3*	58.7	Cone H,d	1.8	1.1	1.6	5.2	15.0	1.4	**2.5×10^{-3}**
213	*13.2p 6.1*	58.7	Cone H,d	1.8	1.1	1.6	5.2	15.0	1.5	**4.3×10^{-4}**
214	*d60-v7-3*	58.7	Cone H,d	1.7	1.1	1.6	7.0	15.0	1.5	**6.5×10^{-2}**
215	*d60-v7-2*	58.7	Cone H,d	1.8	1.1	1.6	7.0	15.0	1.5	**4.6×10^{-2}**
216	*d60-v7-1*	58.7	Cone H,d	1.8	1.1	1.6	7.0	15.0	1.6	**5.7×10^{-1}**
217	*d60-v8,5-3*	58.7	Cone H,d	1.8	1.1	1.6	8.4	15.0	1.4	**3.0×10^{-1}**
218	*d60-v8,5-1*	58.7	Cone H,d	1.8	1.1	1.6	8.5	15.0	1.5	**9.6×10^{-1}**
219	*d60-v8,5-2*	58.7	Cone H,d	1.8	1.1	1.6	8.6	15.0	1.5	**9.5×10^{-1}**
220	*12.11p 9.1*	58.7	Cone H,d	1.5	0.0	0	9.4	2.0	2.4	**9.6×10^{-1}**
221	*12.11p 2.1*	58.7	Cone H,d	1.5	1.1	1.6	9.6	2.0	0.5	**9.8×10^{-1}**
222	*16.4p - 10.1*	58.7	Cone H,d	1.8	0.0	0	9.8	60.0	0.3	**9.6×10^{-1}**
223	*12.11p 4.1*	58.7	Cone h,D	2.0	1.1	0	9.8	60.0	2.7	**9.6×10^{-1}**
224	*16.4p - 12.1*	58.7	Cone H,d	1.8	1.1	0	9.9	0.5	14.5	**2.2×10^{-1}**
225	*16.4p - 16.1*	58.7	Cone H,d	1.7	1.1	12.5	9.9	0.5	14.5	**9.6×10^{-1}**
226	*16.4p - 14.1*	58.7	Cone H,d	1.8	0.0	12.5	10.0	0.5	0.5	**8.6×10^{-1}**
227	*d60-v13,5-1*	58.7	Cone H,d	1.7	1.1	1.6	13.5	15.0	1.5	**9.7×10^{-1}**

with:

- d_{50}: Median particle diameter of Al_2O_3 powder used (µm),
- Pile shape: Dimensions of Cone h, D and H, d of volume 3 cm^3 in
  - Height: h = 8.9 mm and H = 12.7 mm,
  - Diameter: D = 36 mm and d = 30 mm,
- Dimensions of the disc of volume 3 cm^3 in
  - Height: 2.7 mm,
  - Diameter: 38 mm,
- Dimensions of the truncated pyramid of volume 3 cm^3 in
  - Height: 7.3 mm,
  - Sides of base: 25 and 15 mm,

ρ_{pile}: Tap density of powder (g/cm^3),
H_2O: H_2O content (mgH_2O/g),
Rug_{SE}: Roughness of test surface (µm):
V: Free-stream velocity (m/s),
Δt: Duration of exposure to airflow (min),
α: Initial airflow acceleration (m/s^2),
K_R: Resuspension fraction (dimensionless).

The friction velocity v* is calculated from the free-stream velocity V according to the relation:

$$v_* = 0{,}07.V^{0{,}87}$$

The experiments were carried out at temperatures of 24 ± 8° C and at relative humidities of 44 ± 26% RH.